A new juvenile *Yamaceratops* (Dinosauria, Ceratopsia) from the Javkhlant Formation (Upper Cretaceous) of Mongolia

Minyoung Son [1], **Yuong-Nam Lee** [Corresp., 1], **Badamkhatan Zorigt** [2], **Yoshitsugu Kobayashi** [3], **Jin-Young Park** [1], **Sungjin Lee** [1], **Su-Hwan Kim** [1], **Kang-Young Lee** [4]

[1] School of Earth and Environmental Sciences, Seoul National University, Seoul, South Korea

[2] Institute of Paleontology, Mongolian Academy of Sciences, Ulaanbaatar, Mongolia

[3] Hokkaido University Museum, Hokkaido University, Sapporo, Japan

[4] Department of Physics Education, Gyeongsang National University, Jinju, South Korea

Corresponding Author: Yuong-Nam Lee
Email address: ynlee@snu.ac.kr

Here we report a new articulated skeleton of *Yamaceratops dorngobiensis* (MPC-D 100/553) from the Khugenetjavkhlant locality at the Shine Us Khudag (Javkhlant Formation, ?Santonian-Campanian) of the eastern Gobi Desert, Mongolia, which represents the first substantially complete skeleton and the first juvenile individual of this taxon. The specimen includes a nearly complete cranium and large portions of the vertebral column and appendicular skeleton. Its skull is about 2/3 the size of the holotype specimen, based on mandibular length. Its juvenile ontogenetic stage is confirmed by multiple indicators of skeletal and morphological immaturity known in ceratopsians, such as the long-grained surface texture on the long bones, the smooth external surface on the postorbital, open neurocentral sutures of all caudal vertebrae, a large orbit relative to the postorbital and jugal, the low angle of the lacrimal ventral ramus relative to the maxillary teeth row, narrow frontal, and straight ventral edge of the dentary. Osteohistological analysis of MPC-D 100/553 recovered three lines of arrested growth, implying around three years of age when it died, and verifying the immature ontogenetic stage of this specimen. The specimen adds a new autapomorphy of *Yamaceratops*, the rostroventral margin of the fungiform dorsal end of the lacrimal being excluded from the antorbital fossa. Furthermore, it shows a unique combination of diagnostic features of some other basal neoceratopsians: the ventrally hooked rostral bone as in *Aquilops americanus* and very tall middle caudal neural spines about or more than four times as high as the centrum as in *Koreaceratops hwaseongensis*, *Montanoceratops cerorhynchus*, and *Protoceratops andrewsi*. The jugal with the subtemporal ramus deeper than the suborbital ramus as in the holotype specimen is also shared with *Liaoceratops yanzigouensis*, *A. americanus*, and juvenile *P. andrewsi*. Adding 36 new scorings into the recent comprehensive data matrix of basal Neoceratopsia and taking into account the ontogenetically variable characters

recovered *Y. dorngobiensis* as the sister taxon to the Leptoceratopsidae plus Coronosauria. A second phylogenetic analysis with another matrix for Ceratopsia also supported this position. The new phylogenetic position of *Y. dorngobiensis* is important in ceratopsian evolution, as this taxon represents one of the basalmost neoceratopsians with a broad, thin frill and hyper-elongated middle caudal neural spines while still being bipedal.

A new juvenile *Yamaceratops* (Dinosauria, Ceratopsia) from the Javkhlant Formation (Upper Cretaceous) of Mongolia

Minyoung Son[1], Yuong-Nam Lee[1,*], Badamkhatan Zorigt[2], Yoshitsugu Kobayashi[3], Jin-Young Park[1], Sungjin Lee[1], Su-Hwan Kim[1], Kang-Young Lee[4]

[1]School of Earth and Environmental Sciences, Seoul National University, Seoul, South Korea
[2]Institute of Paleontology, Mongolian Academy of Sciences, Ulaanbaatar, Mongolia
[3]Hokkaido University Museum, Hokkaido University, Sapporo, Japan
[4]Department of Physics Education, Gyeongsang National University, Jinju, South Korea

* Corresponding Author: Yuong-Nam Lee
1 Gwanak-ro, Gwanak-gu, Seoul National University, Seoul, 08826, South Korea
Email address: ynlee@snu.ac.kr

ABSTRACT

Here we report a new articulated skeleton of *Yamaceratops dorngobiensis* (MPC-D 100/553) from the Khugenetjavkhlant locality at the Shine Us Khudag (Javkhlant Formation, ?Santonian-Campanian) of the eastern Gobi Desert, Mongolia, which represents the first substantially complete skeleton and the first juvenile individual of this taxon. The specimen includes a nearly complete cranium and large portions of the vertebral column and appendicular skeleton. Its skull is about 2/3 the size of the holotype specimen, based on mandibular length. Its juvenile ontogenetic stage is confirmed by multiple indicators of skeletal and morphological immaturity known in ceratopsians, such as the long-grained surface texture on the long bones, the smooth external surface on the postorbital, open neurocentral sutures of all caudal vertebrae, a large orbit relative to the postorbital and jugal, the low angle of the lacrimal ventral ramus relative to the maxillary teeth row, narrow frontal, and straight ventral edge of the dentary. Osteohistological analysis of MPC-D 100/553 recovered three lines of arrested growth, implying around three years of age when it died, and verifying the immature ontogenetic stage of this specimen. The specimen adds a new autapomorphy of *Yamaceratops*, the rostroventral margin of the fungiform dorsal end of the lacrimal being excluded from the antorbital fossa. Furthermore, it shows a unique combination of diagnostic features of some other basal neoceratopsians: the ventrally hooked rostral bone as in *Aquilops americanus* and very tall middle caudal neural spines about or more than four times as high as the centrum as in *Koreaceratops hwaseongensis*, *Montanoceratops cerorhynchus*, and *Protoceratops andrewsi*. The jugal with the subtemporal ramus deeper than the suborbital ramus as in the holotype specimen is also shared with *Liaoceratops yanzigouensis*, *A. americanus*, and juvenile *P. andrewsi*. Adding 36 new scorings

into the recent comprehensive data matrix of basal Neoceratopsia and taking into account the ontogenetically variable characters recovered *Y. dorngobiensis* as the sister taxon to the Leptoceratopsidae plus Coronosauria. A second phylogenetic analysis with another matrix for Ceratopsia also supported this position. The new phylogenetic position of *Y. dorngobiensis* is important in ceratopsian evolution, as this taxon represents one of the basalmost neoceratopsians with a broad, thin frill and hyper-elongated middle caudal neural spines while still being bipedal.

INTRODUCTION

Ceratopsian dinosaurs appeared in the Late Jurassic of Asia and flourished in the Late Cretaceous of North America. In early evolutionary history, basal ceratopsians were small, bipedal dinosaurs without much-elaborated structures (Xu et al., 2006; Han et al., 2016), but in the Late Cretaceous ceratopsoids, they became quadrupedal giants with large horns and frills on their heads (Sues and Averianov, 2009; Wolfe et al., 2010). Intermediate between the non-neoceratopsian ceratopsians and ceratopsoids are the non-ceratopsoid neoceratopsians, referred to as basal neoceratopsians (You and Dodson, 2004).

The earliest fossil record of ceratopsian dinosaurs appears to be two Jurassic taxa, *Yinlong* and *Hualianceratops*, both from the Upper Jurassic (Oxfordian) Shishugou Formation (Xu et al., 2006; Han et al., 2015; 2016). The transition from basalmost ceratopsians (represented by *Yinlong*) to ceratopsids (represented by *Triceratops*) has encompassed many anatomical innovations through the transformational and step-wise acquisition of unique traits. These include bony structures such as the enlarged frill and horns related to display (Prieto-Márquez et al., 2020), complex dental battery for food processing (Erickson et al., 2015), and even neomorphic ossifications for keratinous coverings such as the rostral, epijugal, epinasal, episquamosal, and epiparietal (Horner and Goodwin, 2008). Ceratopsian evolution is also interesting in obtaining larger body size, bipedal to quadrupedal transition, and dispersal from Asia to Laramidia, Europe, and Appalachia.

Among basal neoceratopsians is *Yamaceratops dorngobiensis* from the Upper Cretaceous Javkhlant Formation of eastern Mongolia (Makovicky and Norell, 2006; Eberth et al., 2009). Although represented by a holotype partial skull and referred disarticulated elements, the exact osteology of *Yamaceratops* was not known yet due to the absence of articulated postcranial skeletons. Thus, the phylogenetic relationships of *Yamaceratops* among basal neoceratopsians have not been entirely solved since its initial description in 2006 (Makovicky and Norell, 2006; Chinnery and Horner, 2007; Makovicky, 2010; Lee et al., 2011; Ryan et al., 2012; Farke et al., 2014; He et al., 2015; Zheng et al., 2015; Han et al., 2018; Knapp et al., 2018; Morschhauser et al., 2018c; Arbour and Evans, 2019; Yu et al., 2020).

Yamaceratops is the only known ceratopsian from the Javkhlant Formation at the Dornogovi Province and its correlative strata at the Zos Canyon locality (Norell and Barta, 2016) (Fig. 1A). Other ceratopsians from the Dornogovi Province of eastern Mongolia include the "psittacosaurs" from the Dzun Shakhai locality (Watabe et al., 2010) and an indeterminate

leptoceratopsid (PIN 4046/11; formerly "*Udanoceratops*") from the Baga Tariach locality (Tereshchenko, 2001; 2020) (Fig. 1B). A *Protoceratops* sp. specimen (MPC-D 100/517) from the Shurg Uul locality is likely from the "Shurguul, Sevrei sum, Omnogovi province," instead of Dornogovi Province (Tsogtbaatar et al., 2019; contra Czepiński, 2020). Some protoceratopsid fossils were reported from the Baga Tariach locality (Watabe et al., 2010), but the specimens had not been described yet.

Ontogeny and variation in a few basal neoceratopsian taxa have been extensively studied since early in research history. It was made possible by discovering many well-preserved specimens from Mongolia, as described by Brown and Schlaikjer (1940) for *Protoceratops andrewsi* and by Maryańska and Osmólska (1975) for *Bagaceratops rozhdestvenskyi*. Despite these studies, many other names have been proposed for specimens of these taxa of different growth stages, especially for juvenile specimens, which were only recently reviewed and synonymized (Makovicky and Norell, 2006; Czepiński, 2019; 2020).

Here we describe a new articulated skeleton of a small individual of *Yamaceratops dorngobiensis* (MPC-D 100/553) discovered from the middle Javkhlant Formation (?Santonian-Campanian) at Khugenetjavkhlant locality in 2014 (Fig. 2, 3). Khugenetjavkhlant is identical to the misspelled 'Khugenslavkhant' (Eberth et al., 2009; Tanaka et al., 2019) and 'Khugenetslavkant' (Makovicky and Norell, 2006; Balanoff et al., 2008; Nesbitt et al., 2011; Makovicky et al., 2011; Varricchio et al., 2015). This is the same locality where the holotype of *Yamaceratops* was found. We found new diagnostic characters for this taxon and described its articulated postcranial skeleton for the first time. We also examined the chronological age of death of this specimen through histological analysis and reviewed the indicators of skeletal and morphological maturity (Hone et al., 2014; 2016; Griffin et al., 2020). Comparing MPC-D 100/553 to the holotype and referred materials, the ontogenetically variable features of *Yamaceratops* were investigated and compared with those in other well-sampled taxa. The well-preserved postcranial anatomy of MPC-D 100/553 offers insight into basal ceratopsian locomotion and evolution as well. We believe that the new osteological characters and inferred patterns of ontogenetic variation in this study can help resolve the phylogenetic position of *Yamaceratops* and understand the character evolution of basal neoceratopsians.

MATERIALS & METHODS

Phylogenetic analysis

A strict consensus tree was constructed based on the most recent iteration of the comprehensive character matrix of Morschhauser et al. (2018c). The Morschhauser et al. (2018c) matrix had 41 taxa with all 257 characters ordered. Later, in the iteration of this matrix by Arbour and Evans (2019), one additional taxon (*Ferrisaurus*) was added, and all characters were treated as unordered, as we followed in this paper. We compared the ontogenetic variation in *Yamaceratops* based on comparisons of the juvenile specimen (MPC-D 100/553) to adult one

(IGM 100/1315) with that of *Protoceratops andrewsi* (Brown and Schlaikjer, 1940) and found generalized patterns. Therefore, we applied them to our analysis, assuming they were widespread in basal neoceratopsians. From these observations, we found additional ontogenetic characters in the Morschhauser et al. (2018c) matrix. They are character numbers 32 and 128, in addition to the previously recognized 8, 53, 58, 59, 98, 162, 177 (Morschhauser et al., 2018c), totaling nine out of 257 characters. Juvenile states in these ontogenetically variable characters were scored as '?' in taxa represented solely by juvenile specimens (*Asiaceratops*, *Aquilops*, '*Graciliceratops*') and *Yamaceratops* (MPC-D 100/553). Although the specimens of *Prenoceratops* were described as immature (Chinnery, 2004b), they were not in the size or morphology that warranted caution, and changing their scores to '?' did not change the resulting topology. The resulting revised scoring of *Yamaceratops* is a total of 36 (character numbers 3, 5, 6, 10, 11, 17, 18, 19, 23, 26, 27, 28, 29, 31, 46, 49, 95, 103, 126, 127, 179, 195, 196, 198, 199, 201, 210, 211, 214, 218, 219, 221, 222, 228, 231, and 236). Additional changes to the scorings were: '[0 1 2]' to '1' for character number 172, '0' to '1' for 178 in *Yamaceratops*, and '?' to '4' for 198 in *Protoceratops andrewsi*. The matrix was analyzed in TNT version 1.5 as parsimony analysis using the Traditional Search (Goloboff and Catalano, 2016). The search followed the method of Morschhauser et al. (2018c) that was iterated in Arbour and Evans (2019), and the parameters are as follows: MaxTrees of 10,000 trees; *Lesothosaurus* as an outgroup taxon; tree bisection reconnection (TBR) swapping algorithm with 1,000 replications.

CT scanning

We made micro-CT scans by using Xradia 620 Versa (Carl Zeiss, USA) for the right jugal (80kV, 127uA, pixel size 56.5881um) and right distal humerus (80kV, 126uA, pixel size 46.6794um), and by using Xradia 520 Versa (Carl Zeiss, USA) for the articulated skull (120kV, 84uA, pixel size 95.2099um). The images were segmented with Dragonfly (Object Research Systems (ORS) Inc., Canada). The scanned images were used to confirm some morphology that is indistinct from the surface of the specimen. Detailed analysis of the internal structure is outside the scope of this paper and will not be discussed here.

Histological analysis

Photography, photogrammetry, and CT scanning of the humerus were conducted before the sectioning. For histologic analysis, we chose associated humerus. Molding and casting were made from the specimen for later research. The mid-shaft of the humerus was sampled for the examination. The sample was prepared and transversely thin sectioned following Lamm (2013). The slides were examined using Nikon Eclipse E600 POL petrographic polarizing microscope with a lambda 530nm plate. The bone cross-section was photographed using a combination of Nikon DS-Ri2 camera and NIS-Elements BR (ver. 4.13) software. Adobe Photoshop (ver. 21.2) is utilized for image enhancement and tracing LAGs. Bone wall thickness and area of the transverse section were quantified by Image J (ver. 1.53).

RESULTS

Systematic paleontology

Dinosauria Owen, 1842 (*sensu* Padian and May, 1993)
Ornithischia Seeley, 1887 (*sensu* Sereno, 1998)
Marginocephalia Sereno, 1986
Ceratopsia Marsh, 1890 (*sensu* Dodson, 1997)
Neoceratopsia Sereno, 1986
Yamaceratops dorngobiensis Makovicky and Norell, 2006

Holotype. IGM 100/1315, an articulated skull from an adult that lacks the rostral, premaxillae, nasals, the predentary, anterior process of the lacrimal, left elements around the temporal region, left posterior mandible, and the parietal (Makovicky and Norell, 2006).

Studied specimen. MPC-D 100/553, a nearly complete articulated skeleton with the left proximal femur and partial foot, but no cervical vertebrae, pectoral girdles, left arm, right hand, other parts of the left leg, and the right foot.

Locality, horizon, and age. Upper Cretaceous (?Santonian-Campanian) Javkhlant Formation, Khugenetjavkhlant, Dornogovi Province, Mongolia.

Emended diagnosis. A neoceratopsian possessing the following autapomorphies: unkeeled rostral bone ventrally hooked and posteriorly expanded; the anteroventral margin of the fungiform anterior process of the lacrimal excluded from the antorbital fossa; jugal with its subtemporal ramus deeper than the suborbital ramus with an angle in between at the ventral edge. In addition, *Yamaceratops dorngobiensis* differs from other basal neoceratopsians by the following unique set of shared characters: a ventrally hooked rostral bone as in *Aquilops americanus*; a fungiform anterior process on the lacrimal as in *Auroraceratops rugosus*; a jugal with a deeper subtemporal ramus than the suborbital ramus as in *Aquilops americanus*, *Liaoceratops yanzigouensis*, and juvenile *Protoceratops andrewsi*; middle caudal neural spines about or more than four times as high as the centrum as in *Koreaceratops hwaseongensis*, *Montanoceratops cerorhynchus*, and *Protoceratops andrewsi*.

Remarks. MPC-D 100/553 is identified as *Yamaceratops* based on the unique characters shared with other *Yamaceratops* specimens (IGM 100/1303 and 100/1315), such as the unkeeled and posteriorly expanded rostral bone, jugal with its subtemporal ramus deeper than the suborbital ramus with an angle in between at the ventral edge, and two tubercles on the ventral margin of the angular (Makovicky and Norell, 2006).

The lacrimal with a “fungiform expansion of the dorsal end” and a “concave rostroventral margin due to limited participation in the floor of the antorbital fossa” was suggested to exist in

Auroraceratops, *Bagaceratops*, and *Liaoceratops* (Morschhauser et al., 2018c). However, the expansion of the anterior ramus is not extensive in *Liaoceratops* (You et al., 2007) and the ventral ramus participates in the medial wall of the antorbital fossa in *Bagaceratops* (Czepiński, 2019). The anterior ramus of the lacrimal is rectangular in *Beg tse* (Yu et al., 2020). Therefore, the fungiform expansion of the anterior ramus of the lacrimal is only distinct in *Auroraceratops* (You et al., 2005) and *Yamaceratops* (MPC-D 100/553). The lacrimal of MPC-D 100/553 differs from *Auroraceratops* and all other basal neoceratopsians. The rostroventral margin of the anterior ramus of the lacrimal neither participates in the floor nor the margin of the antorbital fossa. For these reasons, this character is assigned as an autapomorphy of *Yamaceratops* herein.

The presence and number of angular tubercles are plesiomorphic for basal neoceratopsians, although previously thought to be diagnostic for *Liaoceratops* (Xu et al., 2002) and *Yamaceratops* (Makovicky and Norell, 2006). The numbers and position of the tubercles vary among taxa. Three tubercles are present in *Liaoceratops* (Xu et al., 2002), and two tubercles in *Mosaiceratops* are positioned more dorsally than in *Yamaceratops* (Zheng et al., 2015). However, these are variable in *Auroraceratops*, with the holotype specimen bearing two tubercles on the right angular and none on the left (Morschhauser et al., 2018a). Considering that the tubercles are positioned in the area where the attachment of *M. pterygoideus ventralis* is implied (Nabavizadeh, 2020), these tubercles may result from varying degrees of jaw muscle development. In mammals, similar roughened tubercles are often muscle attachment sites (e.g., Clifford and Witmer, 2004). It is also worth noting that the surangular lateral ridge was suggested as an attachment site of jaw adductor muscle for basal ceratopsians, including *Psittacosaurus* and *Protoceratops* (Haas, 1955; Nabavizadeh, 2020). In *Psittacosaurus* species, the dentary flange well-developed in adults has also been suggested as a site for adductor muscle attachment (Sereno et al., 2010).

Although an embayment at the posterior base of the dorsal process of the jugal is present on both the holotype (IGM 100/1315) and the new specimen of *Yamaceratops* (MPC-D 100/553), this is likely due to postmortem dorsoventral crushing of the skull resulting in the breakage and displacement of the thin dorsal process of the jugal, judging from the micro-CT images of the jugal in MPC-D 100/553. Another possible example of such displacement of the jugal dorsal process due to crushing can be seen in *Aquilops* (Farke et al., 2014).

Ontogenetic Assessment. An osteohistological analysis of the humerus indicates a minimum of three years of chronological age for MPC-D 100/553. It is 2/3 the size of the *Yamaceratops* holotype (IGM 100/1315) based on mandibular length (Makovicky and Norell, 2006). Some indicators of skeletal immaturity seen in MPC-D 100/553 are long-grained surface texture on the long bones (femur, tibia, fibula, humerus, ulna, and radius) (Tumarkin-Deratzian, 2009), the smooth external surface on the postorbital (Brown and Schlaikjer, 1940), and open neurocentral sutures of all caudal vertebrae (Hone et al., 2014).

Description and comparisons

Preservation. The MPC-D 100/553 specimen is nearly complete and articulated in a life-like crouched position. It is dorsoventrally compressed, with the jugal situated about 1.5 cm below its original position based on the surangular ridge. Sediments around the skeleton are carbonate-cemented, contrasting with the poorly-cemented reddish sediment farther from the skeleton. A series of tectonic-induced joints occur across the skeleton, mainly in the left posterior mandible through the right squamosal, humerus, femur, and tibia. The gap is wider along the right leg and is filled with reddish silt.

Skull. The skull (Figs. 4, 5) is mainly articulated, but the left skull roof and most of the left lateral elements posterior to the orbit are not preserved. The occipital region, braincase, and palatal elements are embedded in the matrix. The skull is proportionately much narrower than the holotype (IGM 100/1315). The basal skull length (from the rostral to quadrate articulation) is 111 mm, and the preserved skull length is 142 mm in the sagittal plane. The width of the skull from the sagittal midline to the lateral tip of the epijugal is 53 mm.

Both narial openings, right and partial left orbit, and both antorbital fossa are preserved. The narial opening is oval and anteroventrally oriented 60° to the horizontal plane. It is anteriorly, ventrally, and posteriorly bounded by the premaxilla and dorsally by the nasal. The ventral margin of the narial opening is lower than the anterior tip of the dorsal process of the rostral and the dorsal margin of the antorbital fossa. The posterodorsal end of the narial opening is about the same level as the anteriormost margin of the orbit.

The orbit is large and circular in lateral view. It is dorsally bounded by the prefrontal, frontal, and postorbital in equal proportions. The ventral margin of the orbit is bounded by the lacrimal and jugal. The lacrimal makes up about 17% of the ventral margin of the orbit, while the jugal bounds the rest. The ratio of the orbit to preorbital length is 0.78 (32 mm to 41 mm), which is between the percentages reported for juvenile *Aquilops* (OMNH 34557, 0.84), adult *Archaeoceratops* (IVPP V11114, 0.63), and *Auroraceratops* (CAGS-IG-2004-VD-001, 0.64) (Farke et al., 2014).

The shape and dimension of the infratemporal fenestra cannot be accurately determined, because the ventral process of the squamosal, which articulates with the quadrate, is missing, and the quadrate is directed medially due to the crushing of the skull.

The supratemporal fenestra would have been triangular, given the low curvature of the possible posterior parietal and the squamosal. The right squamosal is medially crushed. The parietal is disarticulated with probable pectoral elements and ribs preserved at the inferred position of the left supratemporal fenestra.

The antorbital fossa is subtriangular in lateral view. It is bounded anteriorly, medially, and ventrally by the maxilla and dorsally by the lacrimal. The fungiform anterior process of the lacrimal does not participate in the antorbital fossa. A deep pocket is ventromedially positioned to the ventral margin of the antorbital fossa, as in *Auroraceratops* (Morschhauser et al., 2018a), juvenile *Protoceratops* (Brown and Schlaikjer, 1940), and *Yamaceratops* (Makovicky and

Norell, 2006). The suture between the maxilla's posterior margin and the lacrimal shaft comprises the posterior margin of the antorbital fossa. The anterior ramus of the jugal contacts but hardly contributes to the posterior margin of the antorbital fossa, as in *Archaeoceratops* (Sullivan & Xu, 2017).

Rostral

The anterior margin of the rostral is unkeeled, making a smooth curved edge similar to *Liaoceratops* (Xu et al., 2002; but see also You and Dodson, 2003) and *Mosaiceratops* (Zheng et al., 2015) among basal neoceratopsians, and chaoyangsaurids and psittacosaurids. In lateral view, the ventral process of the rostral becomes lower in height towards the ventral terminus and curves posteroventrally, forming an almost vertical angle with the posteroventral margin of the rostral and the maxillary tooth row, as in *Aquilops* (Farke et al., 2014). The width of the ventral process tapers anteriorly but not to the extent of a keel (Fig. 5B). It goes at a more acute angle than at the anterior margin of the dorsal process. The lateral surface is slightly convex. The lateral process of the rostral is dorsoventrally low and extends to half-length of the ventral margin of the premaxilla. The dorsal process is slightly expanded posteriorly. The external surface of the rostral is relatively rugose, if not to the extent of anastomosing ridges and grooves as in adult *Yamaceratops* (Makovicky and Norell, 2006).

Premaxilla

Both premaxillae are preserved. In lateral view, it is subrectangular, higher than long, and anteroposteriorly shorter than the maxilla. A shallow fossa is present on the anterodorsal portion of the premaxilla, which forms the anteroventral portion of the narial opening. The ventral margin is slightly convex. The premaxillary-maxillary suture is vertical and dorsally confluent with the posterodorsally inclined premaxillary-lacrimal suture. Although the tip of the posterodorsal process is not fully preserved on both sides, it seems that the premaxilla may have posterodorsally contacted the prefrontal. In palatal view, the premaxilla is mediolaterally widest at the middle.

Maxilla

Both maxillae are well preserved. In lateral view, the maxilla is bounded anterodorsally by the premaxilla, dorsally by the lacrimal, and posteriorly by the jugal. The maxilla bears the whole antorbital fossa with a deep pocket medial to the jugal process. Anterior to the antorbital fossa, the dorsal process receives the expanded anterior process of the lacrimal. The prominent buccal emargination is present along the ventral portion of the jugal process. The emargination converges with the oral margin at the premaxillary-maxillary suture.

Jugal

Only the right jugal is preserved and relatively complete. Only the dorsal tip of the dorsal ramus is missing. In lateral view, the jugal is about twice the length of the orbit (66 mm vs. 32

mm) and comprises the posteroventral corner of the orbit by more than a quarter. The ventral margin of the jugal is convex, with a vertex at about half-length between the anterior and posterior rami.

Along the length of the jugal from the tip of the anterior ramus roughly to the base of the dorsal ramus, the suborbital region of the jugal is laterally convex, making a broad rim around the orbit. Dorsal and ventral to this slight curve, the jugal is essentially flat, except for around the dorsolateral ridge on the posterior ramus. The lateral surface of the jugal is textured as shallow strokes of grooves that are horizontal on the anterior process and vertical on the posterior process. The posterodorsal ridge along the posterolateral edge of the posterior process is also rugose, likely associated with the epijugal in contact and covered with a keratinous sheath as a jugal horn in life.

The anterior ramus of the jugal is anterodorsally curved and dorsoventrally shallow. The mediolateral width of the anterior ramus increases towards the anterior portion of the jugal. The anterodorsal end of the anterior ramus is forked and overlaps the tip of the ventral ramus of the lacrimal. The anterior ramus also anterolaterally contacts the maxilla and ventrally along half its length. It creates a triple point between the maxilla, jugal, and lacrimal at the posterior vertex of the antorbital fossa.

The posterior ramus of the jugal is a bit longer and dorsoventrally deeper than the anterior ramus. The ramus increases in mediolateral width towards the posterior along its suture with the epijugal. The posterior portion of the posterior ramus gently curves downward, as in *Archaeoceratops* (You and Dodson, 2003), *Auroraceratops* (Morschhauser et al., 2018a), juvenile *Bagaceratops* (Czepiński, 2019), *Beg* (Yu et al., 2020), *Liaoceratops* (Xu et al., 2002), *Mosaiceratops* (Zheng et al., 2015), and juvenile *Protoceratops* (Brown and Schlaikjer, 1940). An elongate epijugal is in contact along the posterodorsal ridge on the posterodorsal edge of the posterior ramus. The quadratojugal would have medially met the posterior ramus of the jugal. However, the medial side of the jugal does not show signs of articulation with the quadratojugal. The space between the quadrate and the jugal is occupied by the surangular. It may be due to the dorsoventral crushing of the skull.

The dorsal ramus of the jugal is mediolaterally much thinner than the anterior and posterior ramus. The ventral process of the postorbital covers the anterior part of the dorsal ramus as a scarf joint. It is continuous to the anterior ramus and comprises the posterior margin of the orbit. The posterior part of the dorsal ramus is a thin sheet of bone that forms the anterodorsal margin of the temporal fenestra. In MPC-D 100/553, this bone is positioned medial to the anterodorsal margin of the posterior ramus. The preserved anterodorsal edge of the posterior ramus in the main body of the jugal is horizontal in lateral view and positioned lateral to the posterior part of the dorsal ramus, creating an “embayment” or “notch” (Makovicky and Norell, 2006) at the posterodorsal part of the jugal. The interpretation of the thin bone posterior to the postorbital and medial to the main body of the jugal as a part of the dorsal ramus of the jugal is most parsimonious, given that the dorsal portion of the dorsal ramus of the jugal being expanded posteriorly is a synapomorphy for Neoceratopsia (Butler et al., 2008). This thin sheet

of bone was likely broken and displaced due to postmortem crushing of the skull, as can be confirmed by the absence of contact with the main body of the jugal seen in CT data.

Epijugal

The epijugal is preserved articulated with the posterodorsal ridge of the right jugal. The jugal-epijugal suture is open. The epijugal is gently crescentic, dorsoventrally low, and anteroposteriorly elongate, ranging from the tip of the posterior ramus of the jugal to about halfway up the posterodorsal edge. It does not reach the ventral margin of the jugal, which differs from *Auroraceratops* (Morschhauser et al., 2018a), *Bagaceratops* (Czepiński, 2019), '*Graciliceratops'* (Sereno, 2000), both juvenile and adult *Protoceratops* (Brown and Schlaikjer, 1940), and the holotype specimen of *Yamaceratops* (Makovicky and Norell, 2006). The transverse section of the epijugal is triangular, and its contact with the jugal is concave. The posterolateral tip of the epijugal is rounded. The lateral surface is highly textured, suggesting it was covered with keratin in life as a jugal horn. The jugal horn's posterodorsal position and elongate shape in MPC-D 100/553 are similar to *Leptoceratops, Montanoceratops*, and *Yamaceratops* (Makovicky, 2010).

Nasal

The right nasal is crushed, and the surface is poorly preserved. The nasal comprises the dorsal border of the narial opening and contacts the premaxilla, lacrimal, prefrontal, and frontal. The nasal is flat and mediolaterally wide relative to the frontal. The mediolaterally widest part of the nasal contacts the lacrimal and is almost as wide as the frontal at the contact with the postorbital on the orbital margin (15 mm vs. 16 mm).

Lacrimal

Both left and right lacrimals are preserved. The lacrimal is shaped like a hand ax, with a narrow ventral ramus and greatly expanded anterior ramus. The anterior ramus of the lacrimal is fungiform in lateral view, similar to *Auroraceratops* (You et al., 2005), but unlike the rectangular shape in *Beg* (Yu et al., 2020). It is surrounded by the maxilla ventrally and only meets the premaxilla anterodorsally. Although the point of contact is crushed, the anterior ramus seems to contact the nasal dorsally as in *Archaeoceratops* (You and Dodson, 2003). This condition differs from *Aquilops* (Farke et al., 2014) and *Auroraceratops* (You et al., 2005), which has no contact between the lacrimal and the nasal, and also *Bagaceratops* (Maryańska & Osmólska, 1975), *Leptoceratops* (Sternberg, 1951), and *Protoceratops* (Brown and Schlaikjer, 1940; Lambert et al., 2001), which has an extensive contact between the two bones.

The contact between the premaxilla, nasal, lacrimal, and prefrontal forms a quadruple junction. The anterior ramus of the lacrimal does not contribute to the antorbital fossa. The ventral ramus of the lacrimal is rod-like, similar to *Aquilops* (Farke et al., 2014), *Archaeoceratops* (You and Dodson, 2003), *Auroraceratops* (You et al., 2005), *Leptoceratops* (Sternberg, 1951), and *Liaoceratops* (You et al., 2007). The ventral ramus constitutes the posterodorsal margin of the

antorbital fossa but does not contribute to the medial wall of the antorbital fossa extensively as in protoceratopsids (Brown and Schlaikjer, 1940; Czepiński, 2019). The lacrimal also articulates with the supraorbital, posterior to the posterodorsal contact with the prefrontal.

Prefrontal

The prefrontal is small and relatively thick, contributing to about one-third of the dorsal half of the orbit. The ventral process is posterior to the lacrimal and articulates with the supraorbital. The prefrontal differs from *Bagaceratops* (Czepiński, 2019), *Protoceratops* (Brown and Schlaikjer, 1940), and adult *Yamaceratops* (Makovicky and Norell, 2006), which has an extensive ventral process.

Supraorbital

We follow the term supraorbital, as the bone is homologous in ornithischian dinosaurs instead of "palpebral," which originally refers to a metaplastic ossification in crocodilians (Maidment and Porro, 2010; Nesbitt et al., 2012). Only the right supraorbital is wholly preserved. It is large, with its length reaching half of the orbit. It is elongated and triangular. The supraorbital is articulated with the prefrontal and lacrimal at the base. However, it is collapsed with the tip pointing medioventrally into the orbit, ventral to the collapsed sclerotic ring.

Frontal

The frontal is partially preserved on the right side of the skull. The posterior part, including the frontal fossae and the suture with the parietal, is not preserved. The frontal is flat dorsal to the orbit and gently slopes anteriorly in its contact surface with the nasal. The margin and striations for the contact with the nasal are preserved. In dorsal view, the posteriormost contact with the nasal would have been anterior to the contact with the prefrontal.

Postorbital

The right postorbital is triradiate with the three extremities damaged. The anterior and posterior processes are poorly preserved due to the crushing of the skull, and the narrower ventral process was demarcated by a layer of sediment left in the jugal. The dorsal surface of the postorbital is damaged, and only the anterior margin can be traced. The ventral process would have been narrow and pointed anteroventrally, based on the depression left on the jugal. In the posterodorsal corner of the orbit, the postorbital is divided into the dorsal and lateral surfaces without a distinct ridge. The anterior process at the dorsal surface bounds the posterodorsal corner of the orbit and meets the frontal. The posterior contact with the squamosal is indiscernible and probably damaged, but the preserved length of the postorbital is 33 mm, almost equal to the length of the orbit. The lateral surface of the postorbital is flat and smooth. It is excluded from the infratemporal fenestra by the thin and broad dorsal process of the jugal. The posterior margin of the postorbital is slightly concave and converges with the anterior dorsal process of the jugal.

Squamosal

Only the right squamosal is preserved. Its ventral ramus and the contact with the postorbital, quadrate, and parietal are damaged. In lateral view, the dorsoventral height of the anterior process is highest in the preserved anterior margin. The squamosal tapers towards the posterior margin. The lateral surface is flat to slightly concave. In dorsal view, the squamosal is gently convex laterally, although the transverse width is greatest at the anterior margin due to the lateral crushing of the frill.

Parietal

An isolated element located anteroventral to the right distal fibula is tentatively referred to as the partial posterior margin of the parietal (Fig. 4C). It is long, narrow, generally flat, thin, and slightly curved. It has a low ridge at the dorsal surface, along the concave anterior margin.

Quadrate

The right quadrate is preserved. The condyles are probably in contact with the articular, although obscure. The quadrate head is turned medially, and the pterygoid wing is facing laterally, probably due to the deformation of the skull. There is a straight ridge along the posterolateral edge of the shaft, which is slightly pointed at mid-height.

Braincase

Much of the braincase is incased in the matrix, and detailed analyses from CT data will be presented elsewhere.

Sclerotic ring

A portion of the right sclerotic ring is preserved and exposed, lying on top of the tip of the supraorbital. Three segments can be seen, with the posteroventral ones overlapping the anterodorsal ones. Suppose they represent the original lateral surface of the series. In that case, the exposed portion seems to be from the posterodorsal corner of the sclerotic ring as the center of the ring lies anteroventrally.

Mandible. The right mandible is completely preserved except for around the mandibular fenestra. The left mandible is missing the surangular, and much of the lateral surface is broken.

Predentary

The predentary has a sharp tip and an anteroposteriorly narrow oral margin. The anterior margin is straight and gently keeled. The posteroventral process is bifid from about ventral to the anteroventral corner of the posterior process and ends abruptly at the level of the ventral margin of the dentary. The external surface of the predentary is textured with low grooves and ridges longitudinally radiating from the tip.

Dentary

Both sides of the dentary are preserved. In lateral view, the dentary comprises 59% of the mandible length (54 mm out of 92 mm). The ventral margin of the dentary is relatively straight. The dorsal tip of the coronoid process is textured with rostroventally directed grooves. The dorsal margin of the coronoid process is higher than the dorsal margin of the surangular. The buccal emargination is prominent. The lateral surface of the dentary ventral to the buccal margin is flat and vertical with shallow striations. This condition differs from the laterally flared and striated dentary surface of the holotype of *Yamaceratops* (Makovicky and Norell, 2006).

Surangular

The right surangular is almost complete except for the anteroventral corner. The surangular positions above the angular and behind the dentary. The dorsal margin of the surangular is sinuous with the convex anterior, concave mid-portion, and convex posterior margins. The surangular has a pronounced lateral ridge that is almost horizontal and only slightly inclined posteroventrally. It is laterally highest in the posterior margin and inclines anteriorly. The lateral ridge extends into the dentary, lowering in height. The posteroventral margin of the lateral surface of the surangular is ventrally convex, almost touching the posterior angular tubercle.

Angular

The right angular is almost complete, and the left angular is missing the posterior half of the dorsal and lateroventral portion. It is bifurcate anteriorly along the suture with the dentary and covered by the surangular dorsolaterally. The dorsal margin of the angular is very thin mediolaterally. The lateral surface of the angular is flat and vertical except for the posteriormost part of the angular where the lateral surface faces posteroventrally. The right angular has ventral and posterior tubercles. The ventral tubercle is located dorsolateral to the ventral margin at about mid-length of the angular. The posterior tubercle is located at the posterior quarter, just ventral to the surangular. The ventral tubercle is low and laterally flat, whereas the posterior tubercle is low and dome-shaped. The margin of the mandibular fenestra is damaged but located anterodorsal to the angular.

Dentition. In lateral view, all dentary teeth are covered laterally by the maxillary teeth, and the ventral edges of the maxillary teeth cannot be observed due to the dorsoventral crushing of the skull. However, from the articulated and well-preserved nature of the skull, most, if not all, teeth are likely to be present, as preliminarily seen from the CT images (Fig. 4D). The cingulum is developed on the left maxillary teeth (Jin et al., 2009; *contra* Makovicky and Norell, 2006) (Fig. 5A). Judging from the CT data, there seem to be two premaxillary teeth and nine maxillary and eight dentary teeth with well-developed primary ridges. There is a second row of teeth for replacement.

Overview of the axial elements. The preserved axial column is fully articulated (Figs. 2, 6). The cervical series and most of the dorsal vertebrae are lost due to erosion. The posterior dorsal vertebrae are poorly preserved. The sacral vertebrae are mostly complete, although the contacts are hard to interpret. The anterior caudal vertebrae are in place, although the right transverse processes, right half of the centra, and proximal chevrons are missing. In the transition from the anterior to middle caudal vertebrae, the tail is abruptly turned anteroventrally, with the caudal series still in ascending order with wide spacing. The posterior caudal vertebrae are obscured by the matrix but probably lie ventral to the right tibia and fibula.

Dorsal Vertebrae and Dorsal Ribs

The posterior dorsal vertebrae are preserved, articulated but in poor condition. Their neural spines are lower than those of the anterior caudal vertebrae. The exact morphology of the dorsal vertebrae is hard to observe, as they are fragmented and therefore not fully prepared for stability. The anterior and posterior dorsal ribs are preserved without the proximal portions. The ribs on the right side of the body were probably partially articulated from their respective vertebrae, given they are mostly parallel in the series. The rib cage has collapsed and lie on its left side so that the left ribs lie just below the right ribs. The ribs are long and slender, and the cross-section is oval in the preserved portions.

Sacral Vertebrae and Sacral Ribs

Seven sacral vertebrae are present between the ilia (s1-7). The sacrum is composed of one dorsosacral vertebra (s1), four true sacral vertebrae (s2–s5), and two caudosacral vertebrae (s6–s7). Of the four true sacral vertebrae, s2-4 are medial to the acetabulum. The neural spines of the sacral vertebrae are tilted left, although to a less degree in sacral vertebrae 2-5, so that the right side is primarily exposed in dorsal view. The left side is covered in the matrix, roofed by the neural spines and left ilium. Whether the centra of s1-5 are co-ossified cannot be observed, and the centra of s5-7 are not co-ossified. The pre- and postzygapophyses of s1-8 are poorly developed but not co-ossified. The sacral neural spines are low and anteroposteriorly expanded, widest in s2-5, and the anterior margin is sloping in s6-7. The neural spines are not co-ossified, although the neural spines of s3-4 are in close proximity. From the slight displacement and tilting of both ilia, it can be inferred that the distal ends of the transverse processes nor sacral ribs are not co-ossified with the ilium. The distal ends of the transverse processes are covered on top by the tilted ilium on the right side. However, it is unlikely that the distal ends are co-ossified from the low anteroposterior expansion and wide spacing in the proximal portion. The posterior sacral vertebrae are poorly preserved, and the respective sacral ribs are not preserved.

Caudal Vertebrae, Caudal Ribs, and Chevrons

The anterior to middle caudal vertebrae (cd1-19) are preserved in articulation (Fig. 6A). The more posterior caudal vertebrae are not observable due to the overlying right tibia. There is a slight displacement between the eleventh and twelfth caudal vertebrae following the abrupt turn

of the caudal series (Fig. 6A). All neurocentral sutures are open. In the anteriormost caudal vertebra (cd1), which is located between the posterior ends of the ilia, the anteroposterior width of the neural spine and the length of the centrum is intermediate between the last caudosacral vertebrae (s7) and the second anterior caudal vertebra (cd2). The overlap of zygapophyses is more extensive at the anterior than the middle caudal vertebrae. Overall, the neural spines of the anterior caudal vertebrae are slightly taller and narrower anteroposteriorly than those from the dorsal vertebrae.

The middle caudal vertebrae possess the highest neural spines (preserved in cd13-17) that are much taller and anteroposteriorly narrower than those from the anterior caudal vertebrae (Fig. 6B). In the mid-caudal vertebrae cd17, the height of the preserved neural spine (32 mm) is more than five times the height of its corresponding posterior centrum face (6 mm). It cannot be determined whether the tallest neural spine is at the middle portion of the tail or the more posterior part. The neural spines are gently curved posteriorly, with the base nearly vertical to the centra. The neural spines are only slightly expanded distally. The cross-section of neural spines is oval. The zygapophyses meet nearly horizontally, and each neural arch is tall relative to the centrum. The centra of the middle caudal vertebrae are slightly spool-shaped (waisted), with a concave ventral margin in lateral view. The distal ends of the caudal ribs for the anterior caudal vertebrae are preserved, meeting the ischium (Figs. 2, 6A). They are anteroposteriorly wide and rectangular with parallel anterior and posterior margins headed directly laterally rather than posterolaterally. Caudal ribs are not preserved for the middle caudal vertebrae. The facets for articulation with the caudal ribs are present in cd18, and their presence in more posterior caudal vertebrae cannot be verified. The very tall middle caudal neural spines with the neural spine length about or more than four times the height of the centrum is known in *Koreaceratops hwaseongensis*, *Montanoceratops cerorhynchus*, and *Protoceratops andrewsi* (Tereshchenko, 2008; Lee et al., 2011; Tereshchenko and Singer, 2013). The case for *Bagaceratops* should be taken with caution because the specimen PIN 3143/11, a partial tail, that was referred to and provided data for this taxon (e.g., Tereshchenko, 2007; 2008; Tereshchenko and Singer, 2013) likely instead belongs to *Protoceratops andrewsi* (Czepiński, 2020).

The chevrons of cd11-18 are preserved. The chevrons are rod-like and elongated but much shorter and a bit narrower proximally than the corresponding neural spines. They are wider distally, as in *Leptoceratops* and *Protoceratops andrewsi*, but not as much expanded as in *Auroraceratops* and *Koreaceratops* (Morschhauser et al., 2018b). The chevron is twice as long as the height of the respective centrum face in cd17 (12 mm and 6 mm, respectively).

Ossified Tendons

Three ossified tendons are partially preserved on the right dorsal side of the two anteriormost sacral vertebrae (s1-2). The ossified tendons are parallel to each other and do not overlap. The presence or extent of the ossified tendon is known to be not taxonomically diagnostic because they are subjective to taphonomic biases even among a single basal neoceratopsian taxon from a "geographically and stratigraphically restricted area" (Morschhauser

et al., 2018b). It has been shown that the ossified tendons in hadrosaurine dinosaurs (*Maiasaura peeblesorum* and *Brachylophosaurus canadensis*) were not induced by biomechanical stresses (non-pathologic), and their development began early, as they were even found from a nestling specimen (Adams and Organ, 2005).

Overview of the appendicular elements. Several authors have recently done descriptive and comparative work on the basal ceratopsian appendicular elements for several taxa: they are well described and compared in *Auroraceratops* (Morschhauser et al., 2018b), *Ferrisaurus* (Arbour and Evans, 2019), *Ischioceratops* (He et al., 2015), and *Yinlong* (Han et al., 2018). Juvenile specimens of *Montanoceratops* (Chinnery and Weishampel, 1998) and *Psittacosaurus lujiatunensis* (Hedrick et al., 2014) show a general trend in the ontogeny of basal ceratopsian appendicular elements. This pattern was particularly well described for *Protoceratops andrewsi* (Słowiak et al., 2019) and altogether formed the foundation for comparative work between taxa and ontogenetic stages of specific taxa.

Forelimb. The right humerus, radius, and ulna are preserved articulated (Fig. 7A), although the proximal ulna is missing and the glenoid of the radius is indiscernible.

Humerus

The right humerus is preserved articulated with the ulna and radius. The proximal portion of the humerus is fractured at the proximal end of the deltopectoral crest. The humeral head is covered by overlapping dorsal ribs. The humerus is gracile with less expanded proximal and distal ends and a slender shaft than juvenile *Protoceratops andrewsi* and other basal ceratopsian specimens of more advanced growth stages (Słowiak et al., 2019). It is most similar to '*Graciliceratops*' (ZPAL MgD-I/156). The shaft of the humerus is oval in cross-section as the proximally positioned deltopectoral crest does not extend down to the shaft as a ridge. In *Protoceratops andrewsi*, the cross-section of the humeral shaft is triangular in juveniles (Brown and Schlaikjer, 1940) and distally suboval in young adults (Słowiak et al., 2019). The shaft is slightly bowed posteriorly in lateral view, as in all basal neoceratopsians except *Cerasinops* (Słowiak et al., 2019). The deltopectoral crest is low in lateral view and transversely flat. The overall development of the deltopectoral crest is more similar to *Cerasinops* than *Auroraceratops* and *Protoceratops andrewsi*. In posterior view, the ulnar condyle extends more distally and is transversely narrower than the radial condyle.

Ulna

The distal half of the right ulna is preserved. The cross-section of the ulnar shaft is widely ovated, and its distal end is mediolaterally narrow, likely due to its juvenile state. The distal shaft of the ulna is straight in posterior view, as the general configuration of basal neoceratopsians (Chinnery and Horner, 2007) and in contrast to the medially-bending condition in some leptoceratopsids (*Cerasinops* (MOR 300), *Ferrisaurus* (RBCM P900) *Prenoceratops* (TCM

2003.1.8), and *Udanoceratops* (PIN 3907/11)) (Chinnery, 2004; Chinnery and Horner, 2007; Arbour and Evans, 2019).

Radius

The right radius is preserved except for the proximal end. The mid-shaft is rounded triangular in cross-section as in *Protoceratops andrewsi* and *Auroraceratops* (Słowiak et al., 2019). The lateral margin of the radius is straight.

Pelvic Girdle. The pelvic girdle is well preserved, other than slight displacement and dorsoventral compression during diagenesis.

Ilium

Both ilia are well preserved (Figs. 7B, 8A), only missing the thin anteriormost portions. The pubic peduncles and ischiadic peduncles are partly covered in the matrix. The iliac blade is low and vertical above the acetabulum. In lateral view, the dorsal margin of the ilium is mainly convex but slightly sigmoidal with the preacetabular portion curved anteroventrally with a pivot point dorsal to the pubic peduncle and the posteriormost portion nearly straight but slightly concave with its end curving dorsally. This overall morphology is in line with the referred *Yamaceratops* left ilium of IGM 100/1303, 62% larger than MPC-D 100/553. The postacetabular process of *Yamaceratops* is more elongate than that of most other basal ceratopsians, only rivaled by adult *Protoceratops andrewsi* (e.g., AMNH 6424). The posterior end of the postacetabular process pointing slightly dorsally in *Yamaceratops* resembles the condition of *Mosaiceratops* (*contra* Zheng et al., 2015) and *Protoceratops andrewsi* (Słowiak et al., 2019). The pre- and postacetabular processes are elongated, and the former would not have been much longer than the latter. The postacetabular process is dorsoventrally slightly taller than the preacetabular process. The postacetabular process tapers posteriorly, although this shows ontogenetic or individual variation in *Yinlong* (Han et al., 2018)). The brevis shelf of the postacetabular process is not pronounced. The lateral surface of the ilium is smooth.

The ilium is low above the acetabulum, with the depth of the ilium only half that of the length between the base of the pre- and postacetabular processes. It is unlike other members of Cerapoda but similar to the basal pachycephalosaur (‘heterodontosaurid,’ Dieudonné et al., 2020), *Abrictosaurus*, and the non-neoceratopsian ceratopsians *Stenopelix* and *Yinlong* (Han et al., 2018). The ilium is relatively deeper in the larger specimen of *Yamaceratops* (IGM 100/1303), so this is ontogenetically variable in *Yamaceratops*.

In dorsal view, the dorsal margin of the ilium shows a weak sigmoid curvature where the preacetabular process is slightly laterally deflected, and the postacetabular process is slightly convex laterally. The dorsal margin of the ilium is only slightly everted laterally. The lateral side of the postacetabular process is slightly longitudinally concave.

Ischium

679 The right ischium is exposed, with its medial side facing up, as in dorsoventrally
680 compressed specimens of *Leptoceratops* (CMN 8887; Sternberg, 1951) and juvenile
681 *Protoceratops* (MPC-D 100/530; Fastovsky et al., 2011) (Fig. 7). The end of the pubic peduncle
682 and the iliac peduncle is obscured by the overlying ilium. The ischium is long, dorsoventrally
683 slender, straight, and lacks an obturator process. The ischial shaft is transversely flat, and its
684 medial surface is smooth. The ischial shaft is laterally compressed as in leptoceratopsids such as
685 *Montanoceratops* and *Leptoceratops*, contrary to other basal neoceratopsians where its cross-
686 section is oval (e.g., *Auroraceratops*, *Koreaceratops*, *Mosaiceratops*, and *Protoceratops*
687 *andrewsi*) (Słowiak et al., 2019). The ischium is slightly laterally convex as in *Mosaiceratops*
688 and *Protoceratops*, unlike the straight ischial shaft in *Archaeoceratops* and *Koreaceratops*
689 (Słowiak et al., 2019). The morphology of the ischial shaft is unlikely to be postmortem
690 deformation, as the bone surface shows no sign of breakage from flattening. The distal end is
691 covered in the matrix and lies beneath the caudal vertebrae.
692
693 **Hind Limb.** Both hind limbs are partially preserved (Figs. 2, 7, 8). The right hind limb is
694 preserved articulated and somewhat extended, although the parts distal to the tarsus are not
695 present. The preserved portion of the left hind limb comprises the proximal femur articulated
696 with the ischium and part of the pes.
697
698 Femur
699 The right femur and the proximal one-third of the left femur are preserved. Both femora
700 are articulated with the ilium, so the femoral head could not be seen. The proximal portion of the
701 left femur is only slightly expanded anteroposteriorly. The lesser and greater trochanter is
702 divided by a narrow and shallow groove, but their proximal ends are poorly preserved. The
703 femoral shaft is straight and slender in lateral view. This condition is ontogenetically variable in
704 *Protoceratops andrewsi*, as they are arched in very small juveniles but straight in small to large
705 adults (Słowiak et al., 2019). Only the base of the fourth trochanter is preserved. It is located just
706 proximal to the middle of the femur, facing caudomedially. The existent of fourth trochanter
707 preservation is known to vary with taphonomy among specimens of *Psittacosaurus lujiatunensis*
708 (Hedrick et al., 2014; Persons and Currie, 2019). The inner and outer condyles are obscured by
709 the matrix.
710
711 Tibia
712 Only the right tibia is preserved and is articulated with the fibula and femur. Its posterior
713 surface is exposed in dorsal view. The middle portion of the shaft is missing. The tibia is long
714 and slender, with only modestly expanded ends. At the proximal end, the inner condyle is cut
715 apart by the joint. The distal end of the tibia is laterally expanded to meet the fibula. The distal
716 end of the tibia does not angle medially, as in *Auroraceratops* and *Ischioceratops*, as noted as an
717 exceptional case among non-ceratopsid ceratopsians by Słowiak et al. (2019).
718

Fibula

The right fibula is articulated with the tibia and is also missing the middle portion of the shaft. The proximal end is anteroposteriorly expanded and mediolaterally compressed. The distal fibula is narrow with an oval cross-section. Its distal end curves anteriorly to meet the anterior surface of the distal tibia.

Pes

Only the left pes is preserved and articulated (Fig. 8). The preserved elements are digit Ⅰ to Ⅲ, with only the distal portions of metatarsal Ⅰ to Ⅲ preserved in articulation. The pedal ungual is preserved in digit Ⅲ. The surfaces are broken in the proximolateral surface of phalanx Ⅰ1, the lateral surface of phalanges Ⅰ1 and 2, and the dorsal surfaces of metatarsals Ⅰ to Ⅲ. The first phalanx of digit Ⅰ is longer than that of digit Ⅱ, similar in length to that of digit Ⅲ. The phalanx of digit Ⅰ is narrower than the phalanges of digits Ⅱ and Ⅲ. The second phalanx of digit Ⅱ is shorter than the first but longer than the second phalanx of digit Ⅲ. The phalanx Ⅲ2 is subequal in length but slightly shorter than Ⅲ3.

As in MPC-D 100/553, length of phalanx Ⅱ1 is longer than Ⅱ2 in *Auroraceratops* (Morschhauser et al., 2018b), *Cerasinops* (Gilmore, 1939; Chinnery and Horner, 2007), '*Graciliceratops*' (Maryańska and Osmólska, 1975), *Koreaceratops* (Lee et al., 2011), *Leptoceratops* (Sternberg, 1951), *Montanoceratops* (Chinnery and Weishampel, 1998), *Protoceratops andrewsi* (Brown and Schlaikjer, 1940), *Psittacosaurus amitabha* (Napoli et al., 2019), and indeterminate leptoceratopsid PIN no. 4046/11 (Tereshchenko, 2008; Słowiak et al., 2019),. However, the length of phalanx Ⅱ1 is shorter than Ⅱ2 in *Archaeoceratops* (You and Dodson, 2003) and *Yinlong* (Han et al., 2018).

As in MPC-D 100/553, the length of phalanx Ⅲ2 is subequal to Ⅲ3 in *Ferrisaurus* (Arbour and Evans, 2019), '*Graciliceratops*' (Maryańska and Osmólska, 1975), *Koreaceratops* (Lee et al., 2011), *Protoceratops andrewsi* (Brown and Schlaikjer, 1940), and an indeterminate leptoceratopsid PIN 4046/11 (Tereshchenko, 2008; Słowiak et al., 2019; Arbour and Evans, 2019). The Ⅲ2 are longer than or subequal in length to Ⅲ3 with variable relative lengths in specimens of *Auroraceratops* (Morschhauser et al., 2018b), *Cerasinops*, and *Leptoceratops* (Arbour and Evans, 2019).

The morphology of the pedal ungual is intermediate between hoof-like and claw-like, although its medial and lateral edges and the tip are broken. The proximal end of the pedal ungual is about the same width as the distal end of the preceding pedal phalanx. The relative width of the pedal ungual is known to be ontogenetically variable in *Protoceratops andrewsi* (Słowiak et al., 2019) and even in the ceratopsid *Chasmosaurus belli* (Currie et al., 2016): pedal unguals are relatively longer and narrower in small juveniles than adult-sized individuals. The pedal unguals of two ontogenetic stages of *Yamaceratops* (MPC-D 100/553; IGM 100/1303) are not as elongate as those in some leptoceratopsids (*Cerasinops*, *Ferrisaurus*, *Leptoceratops*), nor

are they broad as those of adult *Protoceratops andrewsi* (Słowiak et al., 2019; Arbour and Evans, 2019).

Bone histology

The humerus of MPC-D 100/553 was examined for histological study (Fig. 9). The cortex of the humerus exhibits longitudinal, reticular, and plexiform vascularization. Four zones are observed. The endosteal region contains a small amount of trabecular bone and plexiform bone matrix with large bone resorption cavities. A small number of radial vessels are observed. Bone vascularity shifts from longitudinal to laminar toward the periosteal region. Bone wall ranges between 2.98-3.64 mm in thickness. The cortex does not contain secondary osteons and active bone remodeling.

The tissue mainly consists of fibro-lamellar. The density of lacunae is less dense in the outer two zones than inside. A total of three lines of arrested growth (LAG) are preserved. In some regions of the cortex, LAGs are obliterated due to taphonomic or diagenetic alterations. The endosteal bone in the humerus is not completed, as in juvenile to sub-adult *Psittacosaurus lujiatunensis* (Zhao et al., 2019). Primary bone remodeling from individuals with three LAGs is also reported from *Psittacosaurus lujiatunensis* and *Psittacosaurus sibiricus* (Zhao et al., 2019; Skutschas et al., 2021), of which erosion bays, the first sign of primary bone remodeling, appeared from this stage.

Instances where the distance between LAGs is decreased in the place where it is expected to increase have been reported for *Psittacosaurus lujiatunensis* (Zhao et al., 2013; 2019). MPC-D 100/553 shows a shorter spacing between the second and third LAG than the first and second LAG like a fibula of *Psittacosaurus lujiatunensis* IVPP V14341.1 with three LAGs (Zhao et al., 2013).

Body size and completeness

MPC-D 100/553 is the smallest and most complete among *Yamaceratops* specimens and the first articulated skeleton (Makovicky and Norell, 2006). Although the presence of additional *Yamaceratops* materials has been mentioned in the literature, they were not described (Eberth et al., 2009; Nesbitt et al., 2011).

Although no detailed measurements were given for other *Yamaceratops* specimens (IGM 100/1315; IGM 100/1303; IGM 100/1867), from the figure, MPC-D 100/553 is 67% the size of the holotype IGM 100/1315 based on the mandibular length and is 62% the size of the referred specimen IGM 100/1303 based on postacetabular length of the ilium. MPC-D 100/553 is slightly smaller than '*Graciliceratops*' ZPAL MgD-I/156 based on the lengths of appendicular elements. Estimation of total body mass of MPC-D 100/553 based on the corrected equation for bipedal animals by Campione et al. (2014) recovered a body mass of 3.5 kg.

Phylogenetic analysis

In the analysis of Arbour and Evans (2019), unordered characters resulted in an extensive polytomy of most non-protoceratopsid basal neoceratopsians without a monophyletic Leptoceratopsidae. The new analysis with updated scorings (42 taxa and 257 characters) that are all unordered recovered both Leptoceratopsidae (except for *Helioceratops* and *Koreaceratops*) and Ceratopsoidea as a monophyletic clade. However, the Protoceratopsidae had collapsed into a polytomy with some of the other basal neoceratopsians.

Removing one unstable taxon, *Helioceratops*, represented by fragmentary materials, resolved this polytomy, yielding a resolved Coronosauria (Protoceratopsidae and Ceratopsoidea) that is a sister clade to Leptoceratopsidae (except *Koreaceratops*), even in the unordered setting. The phylogenetic analysis of 41 taxa and 257 characters produced a strict consensus tree (1160 most parsimonious trees, tree length (TL) = 689 steps) with a topology similar to that of Morschhauser et al. (2018c) but with all characters unordered and no additional steps taken except for removing one unstable taxon (*Helioceratops*). It means that the extensive polytomy from the unordered matrix of Morschhauser et al. (2018c) and Arbour and Evans (2019) has been much resolved. The new analysis for the phylogenetic relationships of *Yamaceratops* within basal neoceratopsians recovered *Yamaceratops* as a sister taxon to the Leptoceratopsidae and Coronosauria combined as suggested by Morschhauser et al. (2018c). The main difference between the two strict consensus trees is the unresolved positions at the base of the tree and the positons of *Asiaceratops*, *Mosaiceratops*, and *Koreaceratops*. The unresolved position between *Hypsilophodon*, *Stegoceras*, and Ceratopsia, and between the Psittacosauridae, Chaoyangsauridae, and Neoceratopsia are expected to some extent since the relevant characters were not the main focus of the matrix by Morschhauser et al. (2018c), and the phylogeny of Cerapoda has not reached a consensus yet (Han et al., 2018; Dieudonné et al., 2020). In a cladogram of Morschhauser et al. (2018c), *Asiaceratops* and *Mosaiceratops* formed a clade with *Yamaceratops* that is a sister clade to the Leptoceratopsidae and Coronosauria combined. In the new analysis, however, only *Yamaceratops* retained this position, and *Asiaceratops* and *Mosaiceratops* are in a position that is more derived than *Liaoceratops* and more basal than *Archaeoceratops*. In addition, in Morschhauser et al. (2018c), *Aquilops* formed a clade with *Auroraceratops* and '*Graciliceratops*' (ZPAL MgD-I/156) between *Archaeoceratops* and the clade including *Yamaceratops*. But in our analysis, the clade has collapsed with the inclusion of *Koreaceratops*.

Removing two taxa, *Helioceratops* and *Koreaceratops* (only known the low body), improved resolution and recovered the previously established monophyletic groups of Leptoceratopsidae, Coronosauria, Protoceratopsidae, and Ceratopsoidea (Fig. 10). The phylogenetic analysis of 40 taxa and 257 characters produced a strict consensus tree (730 most parsimonious trees, tree length (TL) = 688 steps) with a topology again similar to that of Morschhauser et al. (2018c) but with polytomies among basal neoceratopsians resolved. In this iteration, *Asiaceratops* and *Mosaiceratops*, and *Auroraceratops,* and '*Graciliceratops*' (ZPAL

MgD-I/156) formed a clade in their position, and *Aquilops* was recovered as a more derived taxon than the clade of *Auroraceratops* and '*Graciliceratops*' (ZPAL MgD-I/156) and more basal than *Yamaceratops*.

For the conformation of the phylogenetic position of *Yamaceratops*, a second analysis was conducted using the character matrix of Knapp et al. (2018) as iterated by Yu et al. (2020), with only scorings for *Yamaceratops* revised, for 71 taxa with 350 unordered characters using the new technology search algorithm (Fig. 11). The Knapp et al. (2018) matrix encompasses most of the ceratopsid taxon in addition to basal ceratopsians, as opposed to the Morschhauser et al. (2018c) matrix, which is exclusively focused on basal neoceratopsians, with minimal ceratopsids. However, because the Knapp et al. (2018) matrix focused on ceratopsids, many of the characters are on the elaborated frills and horns that are only applicable in ceratopsids. Testing the phylogenetic hypothesis for *Yamaceratops* with the Yu et al. (2020) matrix, the resulting topology is consistent with that of Yu et al. (2020), with paraphyletic Chaoyangsauridae, Psittacosauridae, and Protoceratopsidae. Noticeable differences in the neoceratopsian topology are *Asiaceratops* recovered as a leptoceratopsid, and *Yamaceratops* recovered as the sister taxon to the clade of leptoceratopsids and coronosaurs in the new analysis, both of which were placed as being much basal in the previous result. Compared with our results from the Arbour and Evans (2019) matrix (reiteration of the Morschhauser et al. (2018c) matrix), our new cladogram from the Yu et al. (2020) matrix (reiteration of the Knapp et al. (2018) matrix) recovered a more basal position for *Aquilops* and a more derived position for *Asiaceratops* and '*Graciliceratops*.' Given that these three taxa are known only from juvenile specimens, it seems likely that their positions are subject to changes when ontogenetic variations are considered in the character scorings in the Yu et al. (2020) matrix. Considering juvenile features in scoring the characters from the Knapp et al. (2018) matrix is more complicated because the ontogenetic trajectories of basal neoceratopsians differ from those of ceratopsids, with heterochronic development of derived features (Prieto-Márquez et al., 2020) and should be further studied in the future.

Both of our phylogenetic analyses recovered *Yamaceratops* as the sister taxon to Leptoceratopsidae and Coronosauria combined.

DISCUSSION

Phylogenetic relationships of *Yamaceratops* with other basal neoceratopsians

A new comprehensive phylogenetic analysis including new MPC-D 100/553 recovered *Yamaceratops* as a sister taxon to the Leptoceratopsidae plus Coronosauria.

The thin, narrow, and only slightly curved parietal bar is significant in that in non-ceratopsid ceratopsians, such parietals, indicating the presence of a large parietal foramen, are only known in *Cerasinops* (Chinnery and Horner, 2007) and '*Graciliceratops*' (Sereno, 2000) other than juveniles of more derived protoceratopsids *Protoceratops* (Brown and Schlaikjer,

1940; Handa et al., 2012) and *Bagaceratops* (Czepiński, 2019). The posterior parietals are not thin, and the parietal foramen is small in the more basal *Liaoceratops* (Hu et al., 2002) and *Auroraceratops* (Morschhauser et al., 2018a). The "very slender median and posterior parietal frill margin" similar to MPC-D 100/553 was suggested as a unique character of '*Graciliceratops*' by Sereno (2000) but is known to be ontogenetically variable in *Protoceratops* (Brown and Schlaikjer, 1940; Handa, 2012) and *Bagaceratops* (Czepiński, 2019). From our phylogenetic hypotheses, the presence of a fenestrated frill could have been ancestral for the Leptoceratopsidae and Coronosauria and later lost in leptoceratopsid evolution.

Yamaceratops is the basalmost taxon with the maximum height of the caudal neural spine about or more than four times the height of the associated centrum among basal neoceratopsians, as the phylogenetic position of *Koreaceratops* likely falls within the Leptoceratopsidae (Morschhauser et al., 2018c). It indicates that the tall leaf-shaped tail was perhaps prevalent in leptoceratopsids and protoceratopsids, and later lost in ceratopsids. From the patterns of ontogenetic variation that are concordant in *Yamaceratops* and *Protoceratops*, similar patterns could be expected for other basal neoceratopsians, assuming that they had not diverged, and juvenile specimens could be more reliably incorporated into phylogenetic analyses (Bhullar, 2012).

Bipedalism of *Yamaceratops* (MPC-D 100/553) was predicted based on overall body proportions with long hindlimbs and tested from the quantitative method of Chapelle et al. (2019) using humeral and femoral circumferences. The measured minimum circumference of the humeral shaft is 23 mm, and that of the femoral shaft is 34 mm. Plotting the data to the database of Chapelle et al. (2019) recovered a bipedal to equivocal position close to a juvenile *Psittacosaurus lujiatunensis*. This taxon went from quadrupedal to bipedal during ontogeny. The humeral shaft of MPC-D 100/553 is well preserved, but as the femur had been laterally crushed due to sediment compaction, its circumference is thought to have been slightly shortened. Therefore, assuming the actual minimum femoral circumference was longer than measured, *Yamaceratops* (MPC-D 100/553) fits into the range of bipedal animals. In a recent review, Słowiak et al. (2019) concluded that many skeletal features of *Yinlong*, *Psittacosaurus*, *Liaoceratops*, *Mosaiceratops*, *Archaeoceratops*, and '*Graciliceratops*' were indicative of bipedality, while *Auroraceratops*, *Protoceratops*, and leptoceratopsids were likely mainly quadrupedal, with a possible ontogenetic shift from facultative bipedalism to quadrupedalism in *Protoceratops andrewsi*. Our phylogenetic tree and bipedalism in *Yamaceratops* are mainly congruent with this conclusion.

Ontogenetically variable features in *Yamaceratops*

The number of LAG suggests the relative age of this individual is at least three years old. The humerus contains mainly longitudinal and a small number of reticular and plexiform vessels. Blood vessel organization suggests that bone is mainly growing along its long axis but not very active. Bone circumferential expansion is lagged. The tissue mainly consists of fibro-lamellar, as

observed in modern vertebrates (Horner and Padian, 2004). Based on the absence of the External Fundamental System (Castanet et al., 1988; Ponton et al., 2004; Klein et al., 2009; Woodward et al., 2011), this individual was not somatically mature and was still growing, probably temporarily slowed down.

Although a hierarchical analysis of the ontogeny in *Yamaceratops* is limited at this stage due to the small sample size of two skulls, the new skull offers a glimpse into the indicators of morphological maturity in basal neoceratopsians, as well as features diagnostic for this taxon. MPC-D 100/553 is about 67% the size of the holotype specimen of *Yamaceratops* (IGM 100/1315) based on the mandibular length. Ontogenetically variable features in MPC-D 100/553 concordant with juvenile archosaurs that can be used in Marginocephalia (Griffin et al., 2020) include a relatively large orbit, long-grained surface texture on the femur, tibia, fibula, humerus, ulna, and radius (Tumarkin-Deratzian, 2009), open neurocentral sutures in every caudal vertebra (Brochu, 1996; Hone et al., 2014), ends of the humerus, femur, and tibia composed of poorly-defined, spongy bone (Fastovsky et al., 2011).

Juvenile features of MPC-D 100/553 shared with juvenile specimens of *Yinlong* (Han et al., 2016), *Liaoceratops* (Xu et al., 2002), *Auroraceratops* (You et al., 2012; Morschhauser et al., 2018a; Zhang et al., 2019) *Protoceratops andrewsi* (Brown and Schlaikjer, 1940; Handa et al., 2012; Hone et al., 2014) and *Bagaceratops* (Maryańska and Osmólska, 1975; Czepiński, 2019) include the relatively low angle of the lacrimal ventral ramus relative to the maxillary teeth row, a nasal that is flat and broad relative to the frontal, a relatively small jugal that does not flare laterally with its posterior ramus pointed posteroventrally, postorbital lateral surface smooth, short predentary relative to the dentary length, dentary with a straight ventral edge and flat lateral surface ventral to the buccal emargination, the lateral ridge on the surangular low, and posterior parietal thin and narrow.

The holotype skull of *Yamaceratops* (IGM 100/1315) was described as being from a mature individual, from “closure of the sutures among the occipital and basicranial braincase elements” (Makovicky and Norell, 2006). However, they also noted a possible indicator of immaturity: “the epijugal is not fused to the jugal, a feature that appears to be related to advanced maturity in *Protoceratops andrewsi* and ceratopsids” (Makovicky and Norell, 2006). Compared to MPC-D 100/553, IGM 100/1315 certainly shows features of a more advanced ontogenetic stage: the high angle of the lacrimal ventral ramus relative to the maxillary teeth row; a relatively large jugal that flares laterally, with its posterior ramus pointed posteriorly; postorbital lateral surface rugose; dentary with a ventral edge that is convex in lateral view and curved laterally below the buccal emargination in anterior view; the lateral ridge on the surangular pronounced.

It should be noted that the lateral surangular ridge is well-developed in *Archaeoceratops*, *Bagaceratops*, *Beg*, *Cerasinops*, *Leptoceratops*, *Protoceratops*, and *Yamaceratops* (Makovicky and Norell, 2006; Tanoue et al., 2010; Yu et al., 2020) but very low to absent in *Auroraceratops*, *Liaoceratops*, *Prenoceratops*, *Udanoceratops*, and ceratopsids (Chinnery, 2004a; Makovicky & Norell, 2006; Morschhauser et al., 2018a).

Another variable feature in *Yamaceratops* that is related to ontogeny includes the shape and extent of the epijugal: the epijugal in IGM 100/1315 is crescentic and covers the posterior edge of the jugal to the ventral side (Makovicky and Norell, 2006), whereas the epijugal of MPC-D 100/553 is less curved and only covers the posterodorsal edge of the jugal and does not reach the ventral margin of the jugal. We hypothesize a similar pattern of jugal horn expansion during growth in other ceratopsians with epijugals, although specimens with articulated epijugals are relatively rare.

Many distinctive features in basal neoceratopsian taxa were acquired early in their developmental history, as can be seen from the presence of the additional antorbital fenestra, the edentulous premaxilla, the fused nasals with a distinct bump, and the V-shaped buccal crest in the very immature skull of *Bagaceratops* (ZPAL MgD-I/123) with a medial length of 47 mm (Maryańska and Osmólska, 1975; Czepiński, 2020), all of which are distinguishing features of this taxon. From assessing the maturity of basal neoceratopsian specimens based on comparisons of the two *Yamaceratops* specimens, we decided that the character scorings for *Asiaceratops*, *Aquilops*, and '*Graciliceratops*' had to be revised, following their probable immature status. However, no changes could be made for *Asiaceratops* because no ontogenetically relevant characters had been scored.

Ontogenetic variation in ceratopsians has been described in *Psittacosaurus lujiatunensis*, *Liaoceratops*, *Montanoceratops*, *Protoceratops*, and *Bagaceratops*, but they are either far away from the *Yamaceratops* 'grade' or too fragmentary. Although multiple specimens from a range of ontogenetic stages have been recovered for *Yinlong*, *Psittacosaurus mongoliensis*, and *Auroraceratops*, they had not been studied in detail regarding ontogeny. The discovery of an additional specimen of *Yamaceratops* from an even earlier or much later ontogenetic stage will provide information on the postnatal skeletal development of *Yamaceratops* and add insight into the general patterns of growth in basal neoceratopsian dinosaurs.

Taphonomy

Taphonomic features of MPC-D 100/553 are as follows: (1) stage 0 degree of abrasion with unabraded bones (Fiorillo, 1988; Cook, 1995); (2) stage 1 weathering with bone-cracking from desiccation most apparent on the left lower jaw (Behrensmeyer, 1978; Fiorillo, 1988); (3) absence of root traces, borings, and gnaw/bite marks; (4) transverse/compression fracture breakage pattern (Haynes, 1983) that is most apparent on the right ilium, femur, and tibia; (5) plastic deformation and crushing present; (6) gleying around the skeleton present (Jackson et al., 2018).

The skeletal articulation, crouching posture, and the size of grains in the surrounding matrix (Fig. 2, 12) indicate rapid perimortem to postmortem burial of MPC-D 100/553 (Rogers and Kidwell, 2007) with no transport, and that the carcass did not even float on water (Syme and Salisbury, 2014). A low degree of weathering of the bones and teeth preserved in jaws also

supports limited surface exposure times (Hill, 1980). The bone surfaces show no direct evidence of scavenging.

It is most likely that MPC-D 100/553 was preserved in this state by rapid burial following desiccation upon death. This interpretation is from a series of observations (Fig. 12). MPC-D 100/553 is notable in that: 1) the skeleton lies above a trough cross-bedding of fine- to coarse-grained sandstone with pebbles. 2) The dorsal side of the skeleton is facing the top of the strata. 3) The skeleton is articulated in a life-like crouching or sprawling position with its elbow pointing up. 4) The upper body is curved to the right, and the tail is strongly curved to the right, perpendicular to the pelvis and anterior portion of the tail. 5) The sclerotic ring and the supraorbital have collapsed but are still inside the orbit. 6) An isolated thin and narrow element, likely the posterior portion of the parietal bar, is preserved anteroventral to the distal fibula. 7) The right squamosal is medially compressed with the ribs and probable pectoral elements placed where the left portion of the frill is expected to be, and the cervical series is missing. 8) The ribcage is collapsed, with the right ribs lying above the left ribs, with the ribs above the humeral head. 9) Gleying and carbonate cementation are present around the skeleton. 10) The skeleton is dorsoventrally crushed so that the maxillary teeth cover the dentary teeth, the jugal covers the surangular lateral ridge, the dorsal process of the jugal broken and displaced medially, the postorbital is facing dorsally rather than laterally, legs sprawling with transverse fractures on the femur, ilium disarticulated with its lateral surface facing up, ischium overturned with its medial surface facing up, and the right side of the tail is facing up. 11) Some conjugate tectonic joints cut across the skeleton and the surrounding matrix.

These indicate a taphonomic scenario of death at the lateral accretionary margin of a channel (1, 2, 3), followed by a short period of decay and desiccation of the body leading to breakage of the frill (4, 5, 6, 7, 8), subsequent rapid burial and post-burial microbial activities decomposing the skeleton (9) (Allison, 1988), compression of the skeleton during sediment compaction and diagenesis (10), and final tectonic processes (11). These processes conform to the semi-arid seasonal environment of the middle Javkhlant Formation (Eberth et al., 2009).

MPC-D 100/553 is unlikely to have been preserved inside a burrow because the underlying fine- to coarse-grained sandstone with pebbles and trough cross-bedding (Fig. 12) are indicative of a fluvial deposit that had not been disturbed from burrowing. However, the laterally curved tail of MPC-D 100/553 may have resulted from drying of the carcass during mummification, as has been suggested to have preserved *Auroraceratops* skeletons inside burrows (Suarez et al., 2018). The possibility of miring is also unlikely because of the underlying stratified sandstone without extensive mudstone layers, although MPC-D 100/553 shows the articulation of the skeleton in a life-like crouched posture with flexed hind limbs as in many skeletons preserved from miring (Sander, 1992; Hungerbühler, 1998; Varricchio et al., 2008; Eberth et al., 2010).

The death pose and preservation of MPC-D 100/553 showing dorsoventral compression of the body with the tail turned laterally is likely due to the basal ceratopsian body plan, as can be seen in articulated skeletons of *Psittacosaurus* (SMF R 4970; Mayr et al., 2002),

Koreaceratops (KIGAM VP 200801; Lee et al., 2011), *Leptoceratops* (CMN 8887 and CMN 8888; Sternberg, 1951), *Protoceratops* (e.g., AMNH 7417; Gregory and Mook, 1925), and *Bagaceratops* (MPC-D 100/535; Saneyoshi et al., 2011). *Psittacosaurus sinensis* (IVPP V738) was even preserved in a crouching position with the tail curved (Young, 1958). But in this case, the tail is on top of the leg, unlike the case in MPC-D 100/553, where the right leg is stretched over the curved tail. Such specimens offer insights into post-mortem effects in perfectly articulated specimens.

The state of preservation in MPC-D 100/553 is reminiscent of an articulated *Protoceratops* skeleton (GI SPS 100/512) from the "Fighting Dinosaur" specimen. The *Protoceratops* skeleton GI SPS 100/512 is articulated in a crouching position with its posterior dorsal vertebral column and tail strongly curved and the humeral head placed beneath the ribs (Barsbold, 1974; 2016) as in MPC-D 100/553. Another example of an articulated skeleton with a humeral head placed beneath the dorsal ribs is a partial *Bagaceratops* KID 196 (Kim et al., 2019), although in this case, the scapula and coracoid are articulated with the humerus, all beneath the dorsal ribs. The taphonomy of MPC-D 100/553, GI SPS 100/512, and KID 196 leading to their ribcage over forelimb can mainly be explained through the ventral collapse of the ribcage following decomposition while the shoulder girdle and the forelimb remained relatively in position, resulting in the axial skeleton below the level of articulation with the appendicular skeleton (Carpenter, 1998; Hone et al., 2014). In GI SPS 100/512, from the maxillary teeth preserved below the alveoli and femur disarticulated from the acetabulum, it can be inferred that decay had taken place to a considerable degree (Behrensmeyer and Boaz, 1980) and that the displacement happened after burial, to minimize displacement of disarticulated elements. It is worth noting that the holotype skull of *Yamaceratops* ((IGM 100/1315) also preserves a maxillary tooth outside the alveolus, implying similar taphonomic processes.

A feature listed by Sereno (2010) as an autapomorphy of *Psittacosaurus sinensis* is shared with MPC-D 100/553: "short lower jaw that positions the anterior margin of the predentary in opposition to the premaxilla rather than the rostral." However, the lower jaw in MPC-D 100/553 is more posteriorly positioned relative to the skull than in another *Yamaceratops* specimen IGM 100/1315, and this is likely due to deformation by the dorsoventral compaction of the skull in MPC-D 100/553, while IGM 100/1315 is less deformed (Makovicky and Norell, 2006). There seems to be variation among *Psittacosaurus sinensis* specimens (e.g., IVPP V738 and BNHM BPV149, Sereno, 2010). Moreover, such posteriorly positioned predentary in life is unlikely to have been functionally advantageous for *Psittacosaurus sinensis*, especially given that the premaxillae of *Psittacosaurus* species were edentulous (Sereno, 2010), while in *Yamaceratops,* the premaxillary teeth occluded with the rhamphotheca of the predentary (Figs. 4, 5; Makovicky and Norell, 2006). Therefore, the predentary of *Psittacosaurus sinensis* specimens positioned posterior to the general condition in ceratopsians may also be due to their taphonomy rather than a genuine taxonomic signal.

CONCLUSIONS

A new specimen of *Yamaceratops dorngobiensis* (MPC-D 100/553) was collected at the Khugenetjavkhlant locality from the Upper Cretaceous Javkhlant Formation. MPC-D 100/553 provides essential information on the anatomy of *Yamaceratops,* including autapomorphies which were unknown from the holotype (IGM 100/1315) and referred (IGM 100/1303; IGM 100/1867) specimens of *Yamaceratops*.

The holotype is about 50% larger than the new specimen based on mandibular length. The differences between the holotype and the new specimen, likely representing ontogenetic variation in *Yamaceratops*, were concordant with patterns of ontogenetic variation known in *Protoceratops andrewsi* (Brown and Schlaikjer, 1940). Therefore, MPC-D 100/553 was confirmed as a juvenile. The ontogenetically variable features present in both *Protoceratops* and *Yamaceratops* could be inferred to be shared in basal neoceratopsians or at least in the group that is of intermediate phylogenetic position between *Yamaceratops* and *Protoceratops*.

Histological analysis of the humerus of MPC-D 100/553 recovered three LAGs, indicating around three years old when it died, and confirmed the immature ontogenetic stage of the animal.

The new information on *Yamaceratops* and ontogenetically variable features in basal neoceratopsians recovered from MPC-D 100/553 were used in the new phylogenetic analysis. The analysis recovered *Yamaceratops* as a sister taxon to the Leptoceratopsidae and Coronosauria combined, meaning that *Yamaceratops* is the basalmost taxon with the much-elongated caudal neural spines. During the evolution of ceratopsian dinosaurs, a change occurred in tail morphology, where the neural spines of the middle caudal vertebrae were elongated in basal neoceratopsians, reaching a peak in leptoceratopsids and protoceratopsids, and shortened back in ceratopsids.

INSTITUTIONAL ABBREVIATIONS

AMNH, American Museum of Natural History, New York, USA
CAGS-IG, Chinese Academy of Geological Sciences-Institute of Geology, Beijing, China
CMN, Canadian Museum of Nature, Ottawa, Ontario, Canada
IGM, Institute of Paleontology, Mongolian Academy of Sciences, Ulaanbaatar, Mongolia
IVPP, Institute of Vertebrate Paleontology and Paleoanthropology, Beijing, China
KIGAM VP, Korea Institute of Geoscience and Mineral Resources, Vertebrate Paleontology, Daejeon, Republic of Korea
MOR, Museum of the Rockies, Bozeman, Montana, USA
MPC, Mongolian Paleontological Center, Mongolian Academy of Sciences, Ulaanbaatar, Mongolia
OMNH, Sam Noble Oklahoma Museum of Natural History, Norman, Oklahoma, USA
PIN, Paleontological Institute, Russian Academy of Sciences, Moscow, Russia
RBCM, Royal British Columbia Museum, Victoria, British Columbia, Canada
TCM, The Children's Museum of Indianapolis, Indianapolis, USA

USNM, National Museum of Natural History, Smithsonian Institution, Washington D.C., USA
ZPAL, Zaklad Paleobiologii (Institute of Paleobiology), Polish Academy of Sciences, Warsaw, Poland

ACKNOWLEDGEMENTS

Thanks go to all members of Gobi Dinosaur Supporters in 2014. This research is supported by the National Research Foundation of Korea (Grant Number 2019R1A2B5B02070240) to the corresponding author.

REFERENCES

Adams, J. S., & Organ, C. L. (2005). Histologic determination of ontogenetic patterns and processes in hadrosaurian ossified tendons. *Journal of Vertebrate Paleontology*, *25*(3), 614-622.

Allison, P. A. (1988). The role of anoxia in the decay and mineralization of proteinaceous macro-fossils. *Paleobiology*, 139-154.

Arbour, V. M., & Evans, D. C. (2019). A new leptoceratopsid dinosaur from Maastrichtian-aged deposits of the Sustut Basin, northern British Columbia, Canada. *PeerJ*, *7*, e7926.

Balanoff, A. M., Norell, M. A., Grellet-Tinner, G., & Lewin, M. R. (2008). Digital preparation of a probable neoceratopsian preserved within an egg, with comments on microstructural anatomy of ornithischian eggshells. *Naturwissenschaften*, *95*(6), 493-500.

Barsbold, R. (1974). Duelling dinosaurs. *Priroda* 2, 81−83. [In Russian.]

Barsbold, R. (2016). "The Fighting Dinosaurs": The position of their bodies before and after death. *Paleontological Journal*, *50*(12), 1412-1417.

Behrensmeyer, A.K. (1978). Taphonomic and ecologic information from bone weathering. *Paleobiology*, 4, 150-162.

Behrensmeyer, A. K., & Boaz, D. (1980). The recent bones of Amboseli Park, Kenya, in relation to East African paleoecology. In Behrensmeyer, A. K., & Hill, A. P. (Eds.). (1988). *Fossils in the making: Vertebrate taphonomy and paleoecology*, University of Chicago Press, *69*, 72-92.

Bhullar, B.-A. S. (2012). A phylogenetic approach to ontogeny and heterochrony in the fossil record: cranial evolution and development in anguimorphan lizards (Reptilia: Squamata). *Journal of Experimental Zoology Part B: Molecular and Developmental Evolution*, *318*(7), 521-530.

Brown, B., & Schlaikjer, E. M. (1940). The structure and relationships of *Protoceratops*. *Annals of the New York Academy of Sciences*, *40*(3), 133-266.

Campione, N. E., & Evans, D. C. (2012). A universal scaling relationship between body mass and proximal limb bone dimensions in quadrupedal terrestrial tetrapods. *BMC Biology*, *10*(1), 1-22.

1153 Campione, N. E., Evans, D. C., Brown, C. M., & Carrano, M. T. (2014). Body mass estimation
1154 in non-avian bipeds using a theoretical conversion to quadruped stylopodial
1155 proportions. *Methods in Ecology and Evolution*, *5*(9), 913-923.
1156 Carpenter, K. (1998). Evidence of predatory behavior by carnivorous dinosaurs. *Gaia*, *15*, 135-
1157 144.
1158 Chapelle, K. E., Benson, R. B., Stiegler, J., Otero, A., Zhao, Q., & Choiniere, J. N. (2020). A
1159 quantitative method for inferring locomotory shifts in amniotes during ontogeny, its
1160 application to dinosaurs and its bearing on the evolution of posture. *Palaeontology*, *63*(2),
1161 229-242.
1162 Chinnery, B. (2004a). Description of *Prenoceratops pieganensis* gen. et sp. nov. (Dinosauria:
1163 Neoceratopsia) from the Two Medicine Formation of Montana. *Journal of Vertebrate*
1164 *Paleontology*, *24*(3), 572-590.
1165 Chinnery, B. (2004b). Morphometric analysis of evolutionary trends in the ceratopsian
1166 postcranial skeleton. *Journal of Vertebrate Paleontology*, *24*(3), 591-609.
1167 Chinnery, B. J., & Horner, J. R. (2007). A new neoceratopsian dinosaur linking North American
1168 and Asian taxa. *Journal of Vertebrate Paleontology*, *27*(3), 625-641.
1169 Clifford, A. B., & Witmer, L. M. (2004). Case studies in novel narial anatomy: 2. The enigmatic
1170 nose of moose (Artiodactyla: Cervidae: *Alces alces*). *Journal of Zoology*, *262*(4), 339-360.
1171 Cook, E. (1995). Taphonomy of two non-marine Lower Cretaceous bone accumulations from
1172 southeastern England. *Palaeogeography, Palaeoclimatology, Palaeoecology*, 116,
1173 263e270.
1174 Czepiński, Ł. (2019). Ontogeny and variation of a protoceratopsid dinosaur *Bagaceratops*
1175 *rozhdestvenskyi* from the Late Cretaceous of the Gobi Desert. *Historical Biology*, 1-28.
1176 Czepiński, Ł. (2020). New protoceratopsid specimens improve the age correlation of the Upper
1177 Cretaceous Gobi Desert strata. *Acta Palaeontologica Polonica*, 65(3), 481–497.
1178 Eberth, D. A., Kobayashi, Y., Lee, Y.-N., Mateus, O., Therrien, F., Zelenitsky, D. K., & Norell,
1179 M. A. (2009). Assignment of *Yamaceratops dorngobiensis* and associated redbeds at Shine
1180 Us Khudag (Eastern Gobi, Dorngobi Province, Mongolia) to the redescribed Javkhlant
1181 Formation (Upper Cretaceous). *Journal of Vertebrate Paleontology*, *29*(1), 295-302.
1182 Eberth, D. A., Xing, X. U., & Clark, J. M. (2010). Dinosaur death pits from the Jurassic of
1183 China. *Palaios*, *25*(2), 112-125.
1184 Erickson, G. M., Sidebottom, M. A., Kay, D. I., Turner, K. T., Ip, N., Norell, M. A., Sawyer, W.
1185 G., & Krick, B. A. (2015). Wear biomechanics in the slicing dentition of the giant horned
1186 dinosaur *Triceratops*. *Science Advances*, *1*(5), e1500055.
1187 Farke, A. A., Maxwell, W. D., Cifelli, R. L., & Wedel, M. J. (2014). A ceratopsian dinosaur
1188 from the Lower Cretaceous of western North America, and the biogeography of
1189 Neoceratopsia. *PLOS one*, *9*(12).
1190 Fiorillo, A.R. (1988). Taphonomy of Hazard Homestead Quarry (Ogallala Group), Hitchcock
1191 County, Nebraska. *Contributions to Geology, University of Wyoming*, 26(2), 57-97.

1192 Goloboff, P. A., & Catalano, S. A. (2016). TNT version 1.5, including a full implementation of
1193 phylogenetic morphometrics. *Cladistics*, *32*(3), 221-238.
1194 Granger, W., & Gregory. W. K. (1923). *Protoceratops andrewsi*, a pre-ceratopsian dinosaur
1195 from Mongolia. *American Museum Novitates*, *72*, 1-9.
1196 Gregory, W. K., & Mook, C. C. (1925). On *Protoceratops*, a primitive ceratopsian dinosaur from
1197 the Lower Cretaceous of Mongolia. *American Museum Novitates*, *156*, 1-9.
1198 Haas, G. (1955). The jaw musculature in *Protoceratops* and in other ceratopsians. *American*
1199 *Museum Novitates*, *1729*, 1-24.
1200 Han, F., Forster, C. A., Clark, J. M., & Xu, X. (2015). A new taxon of basal ceratopsian from
1201 China and the early evolution of Ceratopsia. *PloS one*, *10*(12), e0143369.
1202 Han, F.-L., Forster, C. A., Clark, J. M., & Xu, X. (2016). Cranial anatomy of *Yinlong downsi*
1203 (Ornithischia: Ceratopsia) from the Upper Jurassic Shishugou Formation of Xinjiang,
1204 China. *Journal of Vertebrate Paleontology*, *36*(1), e1029579.
1205 Han, F., Forster, C. A., Xu, X., & Clark, J. M. (2018). Postcranial anatomy of *Yinlong downsi*
1206 (Dinosauria: Ceratopsia) from the Upper Jurassic Shishugou Formation of China and the
1207 phylogeny of basal ornithischians. *Journal of Systematic Palaeontology*, *16*(14), 1159-
1208 1187.
1209 Handa, N., Watabe, M., & Tsogtbaatar, K. (2012). New specimens of *Protoceratops*
1210 (Dinosauria: Neoceratopsia) from the Upper Cretaceous in Udyn Sayr, southern Gobi area,
1211 Mongolia. *Paleontological Research*, *16*(3), 179-198.
1212 Haynes, G. (1983). Frequencies of spiral and green-bone fractures on ungulate limb bones in
1213 modern surface assemblages. *American Antiquity*, *48*, 102–114.
1214 He, Y., Makovicky, P. J., Wang, K., Chen, S., Sullivan, C., Han, F., & Xu, X. (2015). A new
1215 Leptoceratopsid (Ornithischia, Ceratopsia) with a unique ischium from the Upper
1216 Cretaceous of Shandong Province, China. *PloS one*, *10*(12).
1217 Hedrick, B. P., Gao, C., Omar, G. I., Zhang, F., Shen, C, & Dodson, P. (2014). The osteology
1218 and taphonomy of a *Psittacosaurus* bonebed assemblage of the Yixian Formation (Lower
1219 Cretaceous), Liaoning, China. *Cretaceous Research*, *51*, 321-340.
1220 Hill, A. P., & Behrensmeyer, A. K. (1980). Early postmortem damage to the remains of some
1221 contemporary East African mammals. In Behrensmeyer, A.K. and Hill, A.P. (Eds.), *Fossils*
1222 *in the making: Vertebrate Taphonomy and Paleoecology*. University of Chicago Press,
1223 Chicago, 131-152.
1224 Hone, D. W., Farke, A. A., & Wedel, M. J. (2016). Ontogeny and the fossil record: what, if
1225 anything, is an adult dinosaur? *Biology Letters*, *12*(2), 20150947.
1226 Horner, J. R., & Goodwin, M. B. (2008). Ontogeny of cranial epi-ossifications in
1227 *Triceratops*. *Journal of Vertebrate Paleontology*, *28*(1), 134-144.
1228 Hungerbühler, A. (1998). Taphonomy of the prosauropod dinosaur *Sellosaurus*, and its
1229 implications for carnivore faunas and feeding habits in the Late Triassic. *Palaeogeography,*
1230 *Palaeoclimatology, Palaeoecology*, *143*(1-3), 1-29.

Jackson, F. D., Zheng, W., Imai, T., Jackson, R. A., & Jin, X. (2018). Fossil eggs associated with a neoceratopsian (*Mosaiceratops azumai*) from the Upper Cretaceous Xiaguan Formation, Henan Province, China. *Cretaceous Research*, *91*, 457-467.

Jin, L., Chen, J., Zan, S., & Godefroit, P. (2009). A new basal neoceratopsian dinosaur from the Middle Cretaceous of Jilin Province, China. *Acta Geologica Sinica-English Edition*, *83*(2), 200-206.

Kim, B., Yun, H., & Lee, Y.-N. (2019). The postcranial skeleton of *Bagaceratops* (Ornithischia: Neoceratopsia) from the Baruungoyot Formation (Upper Cretaceous) in Hermiin Tsav of southwestern Gobi, Mongolia. *Journal of the Geological Society of Korea*, *55*(2), 179-190. [In Korean with English abstract.]

Knapp, A., Knell, R. J., Farke, A. A., Loewen, M. A., & Hone, D. W. (2018). Patterns of divergence in the morphology of ceratopsian dinosaurs: sympatry is not a driver of ornament evolution. *Proceedings of the Royal Society B: Biological Sciences*, *285*(1875), 20180312.

Kurzanov, S. M. (1992). A gigantic protoceratopsid from the Upper Cretaceous of Mongolia. *Paleontological Journal (English version)*, *26*, 103-116.

Lee, Y.-N., Ryan, M. J., & Kobayashi, Y. (2011). The first ceratopsian dinosaur from South Korea. *Naturwissenschaften*, *98*(1), 39-49.

Longrich, N. (2010). The function of large eyes in *Protoceratops*: a nocturnal ceratopsian?. In Ryan, M. J., Chinnery-Allgeier B. J., and Eberth, D.A. (Eds.), *New Perspectives on Horned Dinosaurs: The Royal Tyrrell Museum Ceratopsian Symposium,* Indiana University Press, Bloomington, 308-327.

Maidment, S. C., & Porro, L. B. (2010). Homology of the palpebral and origin of supraorbital ossifications in ornithischian dinosaurs. *Lethaia*, *43*(1), 95-111.

Makovicky, P. J. (2010). A redescription of the *Montanoceratops cerorhynchus* holotype, with a review of referred material. In Ryan, M. J., Chinnery-Allgeier B. J., and Eberth, D.A. (Eds.), *New Perspectives on Horned Dinosaurs: The Royal Tyrrell Museum Ceratopsian Symposium*. Indiana University Press, Bloomington, 68-82.

Makovicky, P. J., & Norell, M. A. (2006). *Yamaceratops dorngobiensis*, a new primitive ceratopsian (Dinosauria: Ornithischia) from the Cretaceous of Mongolia. *American Museum Novitates*, *3530*(1), 1-42.

Makovicky, P. J., Kilbourne, B. M., Sadleir, R. W., & Norell, M. A. (2011). A new basal ornithopod (Dinosauria, Ornithischia) from the Late Cretaceous of Mongolia. *Journal of Vertebrate Paleontology*, *31*(3), 626-640.

Maryańska, T., & Osmólska, H. (1975). Protoceratopsidae (Dinosauria) of Asia. *Palaeontologia Polonica*, *33*, 133-181.

Mayr, G., Peters, S. D., Plodowski, G., & Vogel, O. (2002). Bristle-like integumentary structures at the tail of the horned dinosaur *Psittacosaurus*. *Naturwissenschaften*, *89*(8), 361-365.

Morschhauser, E. M., Li, D., You, H., & Dodson, P. (2018a). Cranial anatomy of the basal neoceratopsian *Auroraceratops rugosus* (Ornithischia: Ceratopsia) from the Yujingzi Basin, Gansu Province, China. *Journal of Vertebrate Paleontology*, *38*(sup1), 36-68.

Morschhauser, E. M., You, H., Li, D., & Dodson, P. (2018b). Postcranial morphology of the basal neoceratopsian (Ornithischia: Ceratopsia) *Auroraceratops rugosus* from the Early Cretaceous (Aptian–Albian) of northwestern Gansu Province, China. *Journal of Vertebrate Paleontology*, *38*(sup1), 75-116.

Morschhauser, E. M., You, H., Li, D., & Dodson, P. (2018c). Phylogenetic history of *Auroraceratops rugosus* (Ceratopsia: Ornithischia) from the Lower Cretaceous of Gansu Province, China. *Journal of Vertebrate Paleontology*, *38*(sup1), 117-147.

Nabavizadeh, A. (2020). Cranial musculature in herbivorous dinosaurs: A survey of reconstructed anatomical diversity and feeding mechanisms. *The Anatomical Record*, *303*(4), 1104-1145.

Nesbitt, S. J., Clarke, J. A., Turner, A. H., & Norell, M. A. (2011). A small alvarezsaurid from the eastern Gobi Desert offers insight into evolutionary patterns in the Alvarezsauroidea. *Journal of Vertebrate Paleontology*, *31*(1), 144-153.

Nesbitt, S. J., Turner, A. H., & Weinbaum, J. C. (2012). A survey of skeletal elements in the orbit of Pseudosuchia and the origin of the crocodylian palpebral. *Earth and Environmental Science Transactions of the Royal Society of Edinburgh*, *103*(3-4), 365-381.

Prieto-Márquez, A., Garcia-Porta, J., Joshi, S. H., Norell, M. A., & Makovicky, P. J. (2020). Modularity and heterochrony in the evolution of the ceratopsian dinosaur frill. *Ecology and Evolution*.

Rogers, R. R., & Kidwell, S. M. (2007). A conceptual framework for the genesis and analysis of vertebrate skeletal concentrations. In Rogers, R.R., Eberth, D.A., and Fiorillo, A.R. (Eds.), *Bonebeds: Genesis, Analysis, and Paleobiological Significance*, University of Chicago Press, Chicago, 1-63.

Ryan, M. J., Evans, D. C., Currie, P. J., Brown, C. M., & Brinkman, D. (2012). New leptoceratopsids from the upper Cretaceous of Alberta, Canada. *Cretaceous Research*, *35*, 69-80.

Sampson, S. D., Ryan, M. J., & Tanke, D. H. (1997). Craniofacial ontogeny in centrosaurine dinosaurs (Ornithischia: Ceratopsidae): taxonomic and behavioral implications. *Zoological Journal of the Linnean Society*, *121*(3), 293-337.

Saneyoshi, M., Watabe, M., Suzuki, S., & Tsogtbaatar, K. (2011). Trace fossils on dinosaur bones from Upper Cretaceous eolian deposits in Mongolia: taphonomic interpretation of paleoecosystems in ancient desert environments. *Palaeogeography, Palaeoclimatology, Palaeoecology*, *311*(1-2), 38-47.

Sander, P. M. (1992). The Norian *Plateosaurus* bonebeds of central Europe and their taphonomy. *Palaeogeography, Palaeoclimatology, Palaeoecology*, *93*(3-4), 255-299.

Schmitz, L., & Motani, R. (2011). Nocturnality in dinosaurs inferred from scleral ring and orbit morphology. *Science*, *332*(6030), 705-708.

Sereno, P. C. (2000). The fossil record, systematics and evolution of pachycephalosaurs and ceratopsians from Asia. In Benton, M.J., Shishkin, M.A., Unwin, D.M., Kurochkin, E.N. (Eds.), *The Age of Dinosaurs in Russia and Mongolia*, Cambridge University Press, Cambridge, 480-516.

Sereno, P. C. (2010). Taxonomy, cranial morphology, and relationships of parrot-beaked dinosaurs (Ceratopsia: Psittacosaurus). In Ryan, M. J., Chinnery-Allgeier B. J., and Eberth, D.A. (Eds.), *New perspectives on horned dinosaurs: The Royal Tyrrell Museum ceratopsian symposium*, Indiana University Press, Bloomington, 21-58.

Skutschas, P.P., Morozov, S.S., Averianov, A.O., Leshchinskiy, S.V., Ivantsov, S.V., Fayngerts, A.V., Feofanova, O.A., Vladimirova, O.N., and Slobodin, D.A. (2021). Femoral histology and growth patterns of the ceratopsian dinosaur *Psittacosaurus sibiricus* from the Early Cretaceous of Western Siberia. *Acta Palaeontologica Polonica*, *66*(2), 437-447.

Słowiak, J., Tereshchenko, V. S., & Fostowicz-Frelik, Ł. (2019). Appendicular skeleton of *Protoceratops andrewsi* (Dinosauria, Ornithischia): comparative morphology, ontogenetic changes, and the implications for non-ceratopsid ceratopsian locomotion. *PeerJ*, 7, e7324.

Suarez, C. A., Morschhauser, E. M., Suarez, M. B., You, H., Li, D., & Dodson, P. (2018). Rare earth element geochemistry of bone beds from the Lower Cretaceous Zhonggou Formation of Gansu Province, China. *Journal of Vertebrate Paleontology*, *38*(sup1), 22-35.

Sues, H. D., & Averianov, A. (2009). *Turanoceratops tardabilis*—the first ceratopsid dinosaur from Asia. *Naturwissenschaften*, *96*(5), 645-652.

Sullivan, C., & Xu, X. (2017). Morphological diversity and evolution of the jugal in dinosaurs. *The Anatomical Record*, *300*(1), 30-48.

Syme, C. E., & Salisbury, S. W. (2014). Patterns of aquatic decay and disarticulation in juvenile Indo-Pacific crocodiles (*Crocodylus porosus*), and implications for the taphonomic interpretation of fossil crocodyliform material. *Palaeogeography, Palaeoclimatology, Palaeoecology*, *412*, 108-123.

Tanaka, K., Kobayashi, Y., Zelenitsky, D. K., Therrien, F., Lee, Y.-N., Barsbold, R., ... & Idersaikhan, D. (2019). Exceptional preservation of a Late Cretaceous dinosaur nesting site from Mongolia reveals colonial nesting behavior in a non-avian theropod. *Geology*, *47*(9), 843-847.

Tereshchenko, V. S. (2007). Key to protoceratopoid vertebrae (Ceratopsia, Dinosauria) from Mongolia. *Paleontological Journal*, *41*(2), 175-188.

Tereshchenko, V. S. (2008). Adaptive features of protoceratopoids (Ornithischia: Neoceratopsia). *Paleontological Journal*, *42*(3), 273-286.

Tereshchenko, V. S., & Singer, T. (2013). Structural features of neural spines of the caudal vertebrae of protoceratopoids (Ornithischia: Neoceratopsia). *Paleontological Journal*, *47*(6), 618-630.

Tumarkin-Deratzian, A. R. (2009). Evaluation of long bone surface textures as ontogenetic indicators in centrosaurine ceratopsids. *The Anatomical Record*, *292*(9), 1485-1500.

Varricchio, D. J., Sereno, P. C., Xijin, Z., Lin, T., Wilson, J. A., & Lyon, G. H. (2008). Mud-trapped herd captures evidence of distinctive dinosaur sociality. *Acta Palaeontologica Polonica*, *53*(4), 567-578.

Varricchio, D. J., Balanoff, A. M., & Norell, M. A. (2015). Reidentification of avian embryonic remains from the Cretaceous of Mongolia. *PLoS One*, *10*(6), e0128458.

Wolfe, D. G., Kirkland, J. I., Smith, D., Poole, K., Chinnery-Allgeier, B. J., & McDonald, A. (2010). *Zuniceratops christopheri*: The North American ceratopsid sister taxon reconstructed on the basis of new data. In Ryan, M. J., Chinnery-Allgeier B. J., and Eberth, D.A. (Eds.), *New perspectives on horned dinosaurs: The Royal Tyrrell Museum Ceratopsian Symposium*. Indiana University Press, Bloomington, 91-98.

Xu, X., Forster, C. A., Clark, J. M., & Mo, J. (2006). A basal ceratopsian with transitional features from the Late Jurassic of northwestern China. *Proceedings of the Royal Society B: Biological Sciences*, *273*(1598), 2135-2140.

You, H.-L., & Dodson, P. (2003). Redescription of neoceratopsian dinosaur *Archaeoceratops* and early evolution of Neoceratopsia. *Acta Palaeontologica Polonica*, *48*(2),261-272.

You, H.-L., & Dodson, P. (2004). Basal Ceratopsia. In: Weishampel, D.B., Dodson, P., & Osmólska, H. (eds.), *The Dinosauria, Second Edition*. University of California Press, Berkeley, 478–493.

You, H., Li, D., Ji, Q., Lamanna, M. C., & Dodson, P. (2005). On a new genus of basal neoceratopsian dinosaur from the Early Cretaceous of Gansu Province, China. *Acta Geologica Sinica*, *79*(5), 593-597.

Young, C.C. (1958). The dinosaurian remains of Laiyang, Shantung, *Palaeontologica Sinica*, New Series C, 16, 53-138.

Yu, C., Prieto-Marquez, A., Chinzorig, T., Badamkhatan, Z., & Norell, M. (2020). A neoceratopsian dinosaur from the early Cretaceous of Mongolia and the early evolution of ceratopsia. *Communications biology*, *3*(1), 1-8.

Zhao, Q., Benton, M. J., Sullivan, C., Sander, P. M., & Xu, X. (2013). Histology and postural change during the growth of the ceratopsian dinosaur *Psittacosaurus lujiatunensis*. *Nature communications*, *4*(1), 1-8.

Zhao, Q., Benton, M. J., Hayashi, S., & Xu, X. (2019). Ontogenetic stages of ceratopsian dinosaur *Psittacosaurus* in bone histology. *Acta Palaeontologica Polonica*, *64*(2).

Zheng, W., Jin, X., & Xu, X. (2015). A psittacosaurid-like basal neoceratopsian from the Upper Cretaceous of central China and its implications for basal ceratopsian evolution. *Scientific reports*, *5*, 14190.

Figure captions

Figure 1 Maps of the locality where the new skeleton of *Yamaceratops dorngobiensis* (MPC-D 100/553) was discovered. (A) Map of Mongolia. Stars represent the outcrops of the Javkhlant Formation and its correlative strata; green star indicates the Zos Canyon locality and red star the Khugenetjavkhlant locality; (B) Map of Dornogovi Province. Red stars indicate ceratopsian localities. Yellow stars represent the main localities of the Bayanshiree Formation. Dashed lines represent province boundaries.

Figure 2 Skeleton of *Yamaceratops dorngobiensis* (MPC-D 100/553) in right dorsolateral view. (A) Photograph; (B) Interpretive drawing. Bones are bounded by solid lines and colored beige; matrix is gray. Shaded areas represent the broken surface of bones. Abbreviations: cd, caudal vertebrae; dr, dorsal ribs; dv, dorsal vertebrae; f, femur; fi, fibula; h, humerus; L, bone on the left side; p, isolated parietal; pp, pedal phalanges; R, bone on the right side; ra, radius; sk, skull; sv, sacral vertebrae; ti, tibia; u, ulna; il, ilium; is, ischium.

Figure 3 Skeletal reconstruction of juvenile *Yamaceratops dorngobiensis* (MPC-D 100/553) in right lateral view. (A) Reconstruction of the skeleton with preserved parts colored in white and missing bones in gray; (B) Reconstruction of the complete skeleton, restored based on other basal neoceratopsian skeletons.

Figure 4 Skull of *Yamaceratops dorngobiensis* (MPC-D 100/553). (A) Photograph and (B) interpretive drawing in right lateral view; (C) isolated parietal fragment in dorsal view; (D) posterior mandible in right lateral view; (E) longitudinal micro-CT cross section of the skull. Abbreviations: a, angular; aof, antorbital fossa; at, angular tubercle; d, dentary; dr, dorsal ribs; ej, epijugal; fr, frontal; j, jugal; L, bone on the left side; la, lacrimal; mx, maxilla; mxt, maxillary tooth; n, nasal; p, isolated parietal; pd, predentary; pmt, premaxillary tooth; pmx, premaxilla; po, postorbital; prf, prefrontal; q, quadrate; R, bone on the right side; r, rostral.

Figure 5 Skull of *Yamaceratops dorngobiensis* (MPC-D 100/553) in (A) left lateral and (B) anterior view. Abbreviations: a, angular; aof, antorbital fossa; d, dentary; f (R), right femur; fr, frontal; h, humerus; j, jugal; la, lacrimal; mx, maxilla; n, nasal; pd, predentary; pf, prefrontal; pmt, premaxillary tooth; pmx, premaxilla; po, postorbital; prf, prefrontal; r, rostral; ra, radius; sq, squamosal; sa, surangular; scl, sclerotic ring; so, supraorbital; u, ulna.

Figure 6 Axial skeleton of *Yamaceratops dorngobiensis* (MPC-D 100/553). (A) dorsal to anterior caudal vertebrae in right lateral view; (B) middle caudal vertebrae with very tall

neural spines in right lateral view. Abbreviations: cd, caudal vertebra; cr, caudal ribs; dv, dorsal vertebrae; s: sacral vertebra; ti, tibia; is, ischium.

Figure 7 Right appendicular skeleton of *Yamaceratops dorngobiensis* (MPC-D 100/553). (A) Forelimb in ventrolateral view; (B) Pelvic girdle and hind limb in lateral view. Abbreviations: dpc, deltopectoral crest; f, femur; fi, fibula; ft, fourth trochanter; gt, greater trochanter; h, humerus; ra, radius; u, ulna. L, bones on the left side; lt, lesser trochanter; R, bones on the right side; ti, tibia; ico, inner condyle of the tibia; il, ilium; is, ischium.

Figure 8 Left appendicular skeleton of *Yamaceratops dorngobiensis* (MPC-D 100/553). (A) Ilium and pes in lateral view; (B) Pes in dorsal view. Abbreviations: f, femur; ft, fourth trochanter; gt, greater trochanter; L, bones on the left side; lt, lesser trochanter; mt, metatarsal; R, bones on the right side; il, ilium; Ⅰ, pedal digit Ⅰ; Ⅱ, pedal digit Ⅱ; Ⅲ, pedal digit Ⅲ.

Figure 9 Histological section of the right humeral shaft of *Yamaceratops dorngobiensis* (MPC-D 100/553). Three LAGs are traced in white lines.

Figure 10 Phylogenetic relationships of *Yamaceratops dorngobiensis* among ceratopsians using the Arbour and Evans (2019) matrix. Strict consensus tree constructed by using the character matrix of Arbour and Evans (2019) (iteration of the Morschhauser et al. (2018c) matrix) with updated scorings for *Yamaceratops dorngobiensis* and ontogenetically variable characters unscored in taxa represented solely by juvenile specimens. Taxa with middle caudal neural spines about or more than four times longer than the centrum height are highlighted as red color. Numbers at each node indicate Bremer support values.

Figure 11 Phylogenetic relationships of *Yamaceratops dorngobiensis* among ceratopsians using the Yu et al. (2020) matrix. Strict consensus tree constructed by using the character matrix of Yu et al. (2020) (iteration of the Knapp et al. (2018) matrix) with updated scorings for *Yamaceratops dorngobiensis*. *Yamaceratops dorngobiensis* is highlighted as red color. Numbers at each node indicate Bremer support values.

Figure 12 Taphonomy of MPC-D 100/553. (A) Photograph of the outcrop at the fossil locality. Red star indicates the position where MPC-D 100/553 was found; (B) Photograph of MPC-D 100/553 exposed at the flank of a hill as found, during the excavation; (C) MPC-D 100/553 (skull removed) and its underlying matrix with bedding preserved. The white lines mark the boundary between coarse- and fine-grained sandstone.

Figure 1

Maps of the locality where the new skeleton of *Yamaceratops dorngobiensis* (MPC-D 100/553) was discovered.

(A) Map of Mongolia. Stars represent the outcrops of the Javkhlant Formation and its correlative strata; green star indicates the Zos Canyon locality and red star the Khugenetjavkhlant locality; (B) Map of Dornogovi Province. Red stars indicate ceratopsian localities. Yellow stars represent the main localities of the Bayanshiree Formation. Dashed lines represent province boundaries.

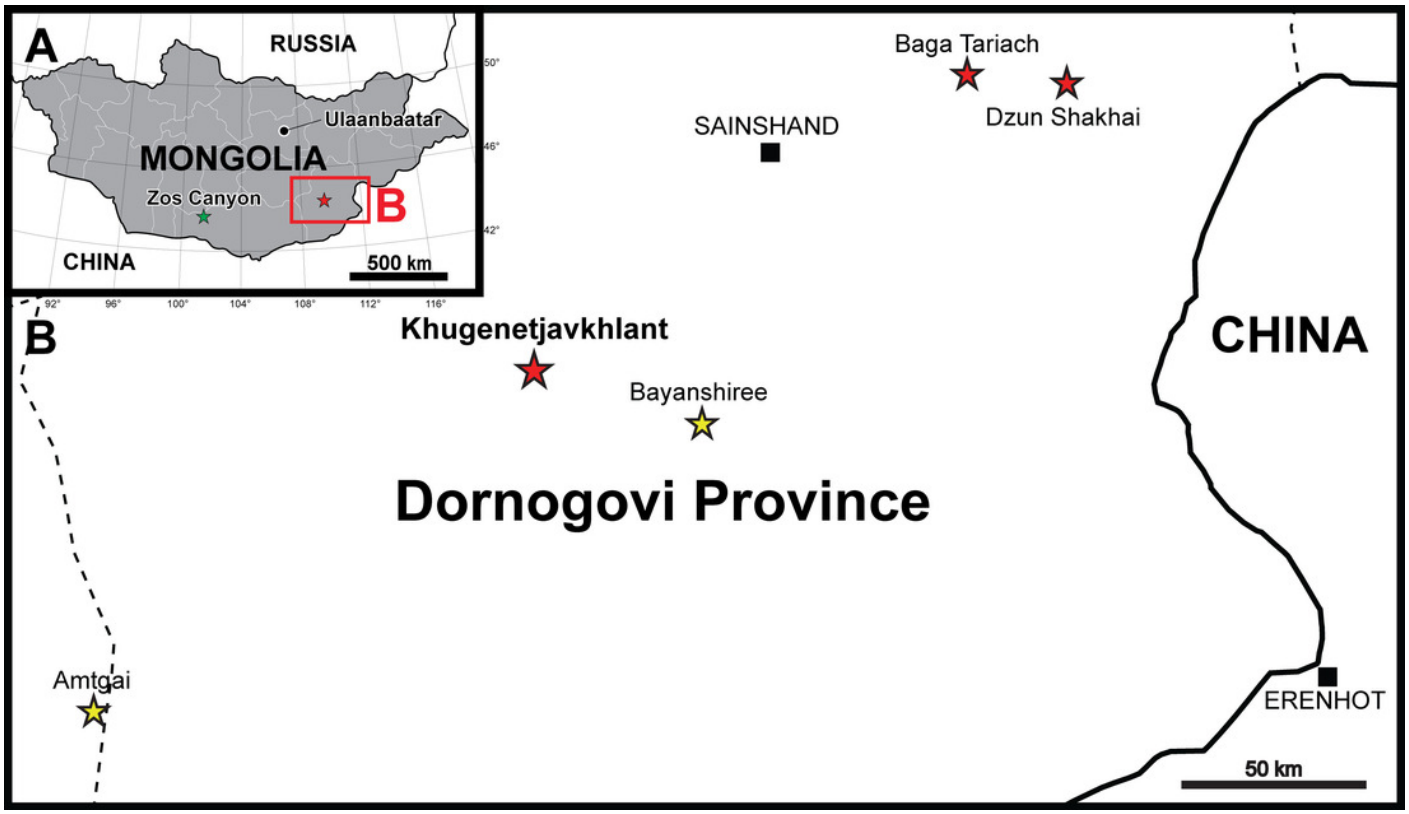

Figure 2

Skeleton of *Yamaceratops dorngobiensis* (MPC-D 100/553) in right dorsolateral view.

(A) Photograph; (B) Interpretive drawing. Bones are bounded by solid lines and colored beige; matrix is gray. Shaded areas represent the broken surface of bones. Abbreviations: cd, caudal vertebrae; dr, dorsal ribs; dv, dorsal vertebrae; f, femur; fi, fibula; h, humerus; L, bone on the left side; p, isolated parietal; pp, pedal phalanges; R, bone on the right side; ra, radius; sk, skull; sv, sacral vertebrae; ti, tibia; u, ulna; il, ilium; is, ischium.

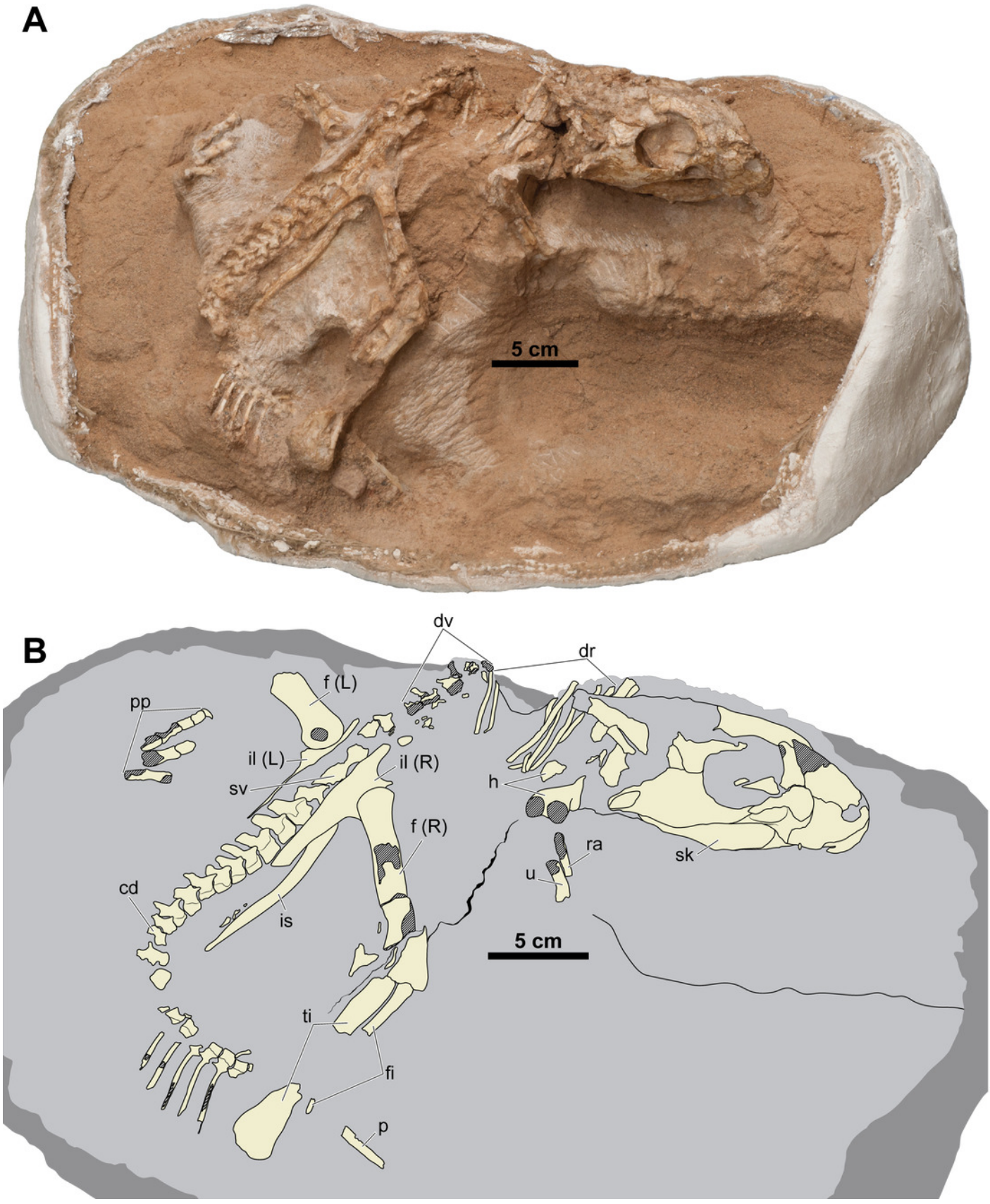
A
5 cm
B
dv
dr
f (L)
pp
il (L)
il (R)
sv
h
f (R)
ra
sk
u
cd
is
5 cm
ti
fi
p

Figure 3

Skeletal reconstruction of juvenile *Yamaceratops dorngobiensis* (MPC-D 100/553) in right lateral view.

(A) Reconstruction of the skeleton with preserved parts colored in white and missing bones in gray; (B) Reconstruction of the complete skeleton, restored based on other basal neoceratopsian skeletons.

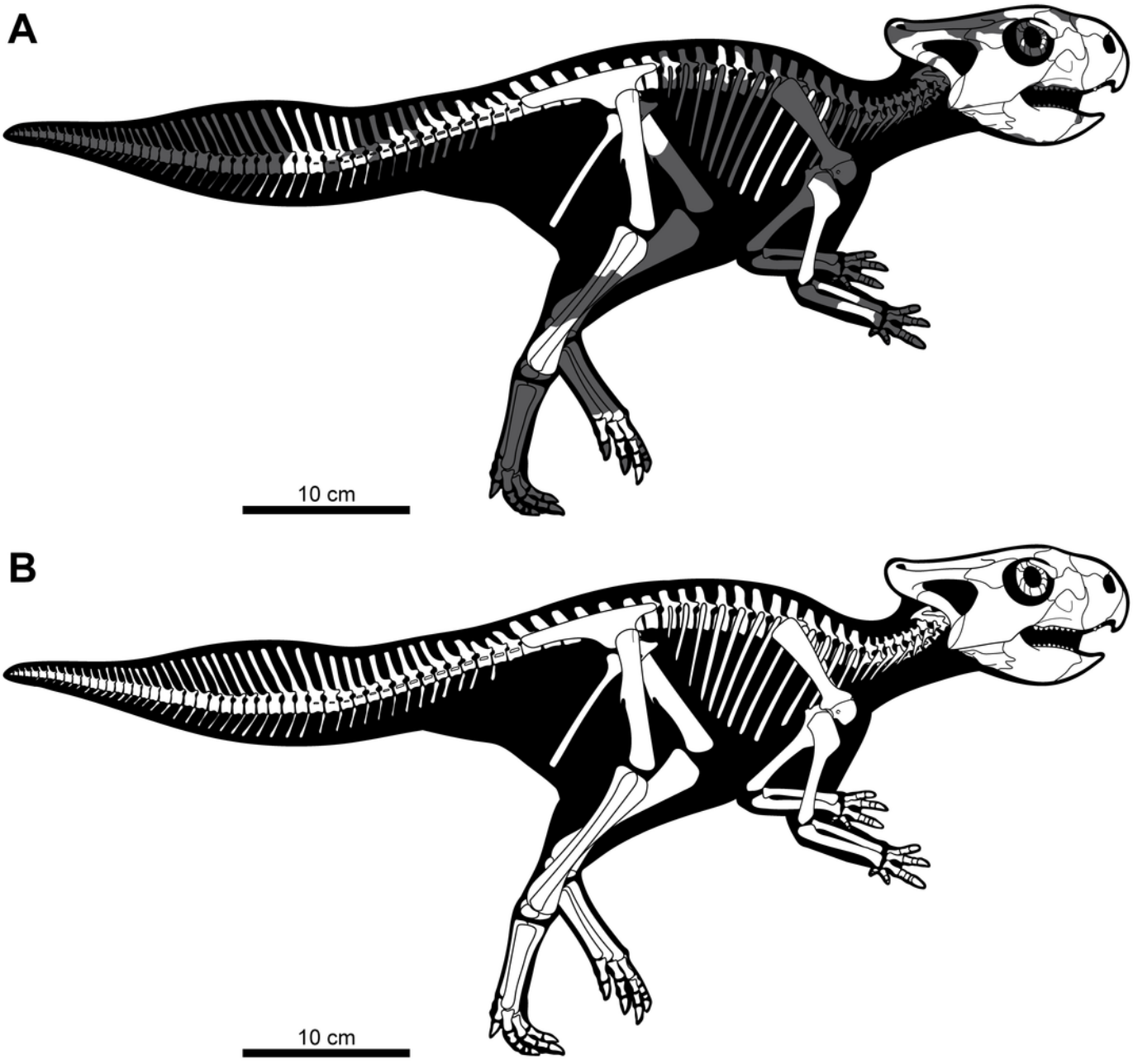
A
10 cm
B
10 cm

Figure 4

Skull of *Yamaceratops dorngobiensis* (MPC-D 100/553).

(A) Photograph and (B) interpretive drawing in right lateral view; (C) isolated parietal fragment in dorsal view; (D) posterior mandible in right lateral view; (E) longitudinal micro-CT cross section of the skull. Abbreviations: a, angular; aof, antorbital fossa; at, angular tubercle; d, dentary; dr, dorsal ribs; ej, epijugal; fr, frontal; j, jugal; L, bone on the left side; la, lacrimal; mx, maxilla; mxt, maxillary tooth; n, nasal; p, isolated parietal; pd, predentary; pmt, premaxillary tooth; pmx, premaxilla; po, postorbital; prf, prefrontal; q, quadrate; R, bone on the right side; r, rostral.

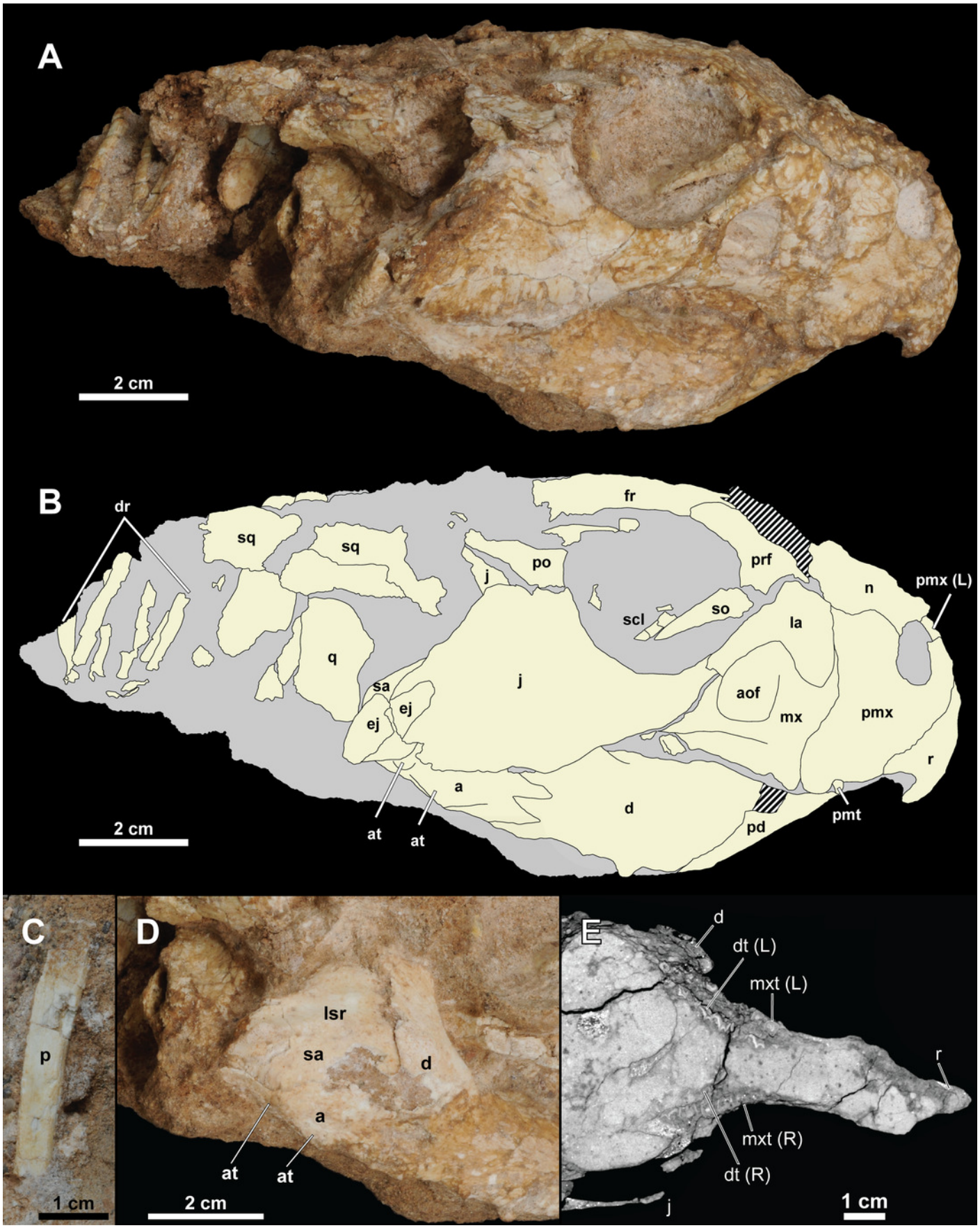
A
2 cm
B
dr
sq
sq
fr
po
prf
j
n
pmx (L)
scl
so
la
q
sa
j
aof
ej
ej
mx
pmx
r
a
d
pd
pmt
2 cm
at
at
C
p
1 cm
D
lsr
sa
d
a
at
at
2 cm
E
d
dt (L)
mxt (L)
r
mxt (R)
dt (R)
j
1 cm

Figure 5

Skull of *Yamaceratops dorngobiensis* (MPC-D 100/553) in (A) left lateral and (B) anterior view.

Abbreviations: a, angular; aof, antorbital fossa; d, dentary; f (R), right femur; fr, frontal; h, humerus; j, jugal; la, lacrimal; mx, maxilla; n, nasal; pd, predentary; pf, prefrontal; pmt, premaxillary tooth; pmx, premaxilla; po, postorbital; prf, prefrontal; r, rostral; ra, radius; sq, squamosal; sa, surangular; scl, sclerotic ring; so, supraorbital; u, ulna.

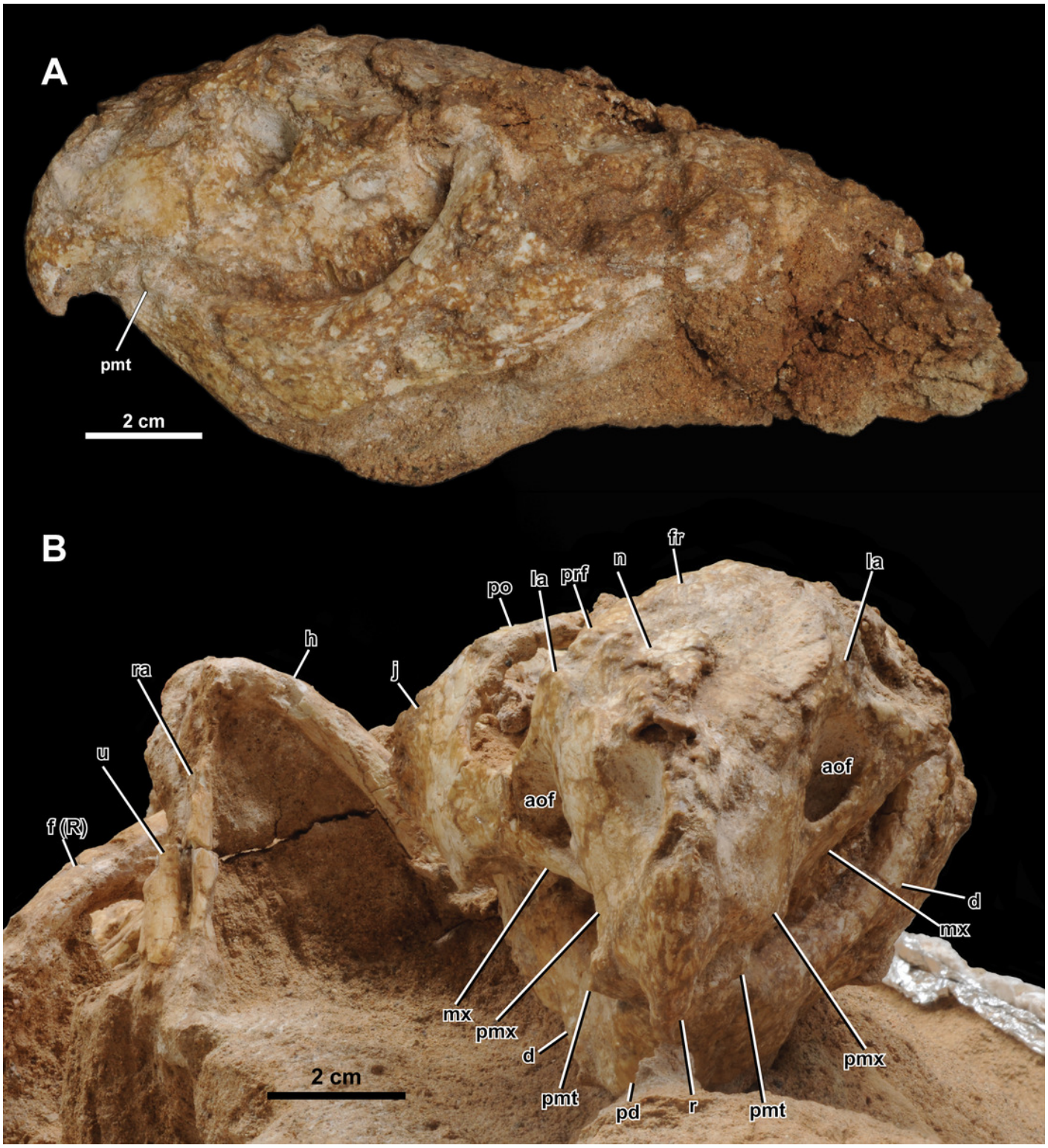
A
pmt
2 cm
B
fr
n
la
po
la
prf
h
ra
j
u
aof
aof
f (R)
d
mx
mx
pmx
d
pmt
pd
r
pmt
pmx
2 cm

Figure 6

Axial skeleton of *Yamaceratops dorngobiensis* (MPC-D 100/553).

(A) dorsal to anterior caudal vertebrae in right lateral view; (B) middle caudal vertebrae with very tall neural spines in right lateral view. Abbreviations: cd, caudal vertebra; cr, caudal ribs; dv, dorsal vertebrae; s: sacral vertebra; ti, tibia; is, ischium.

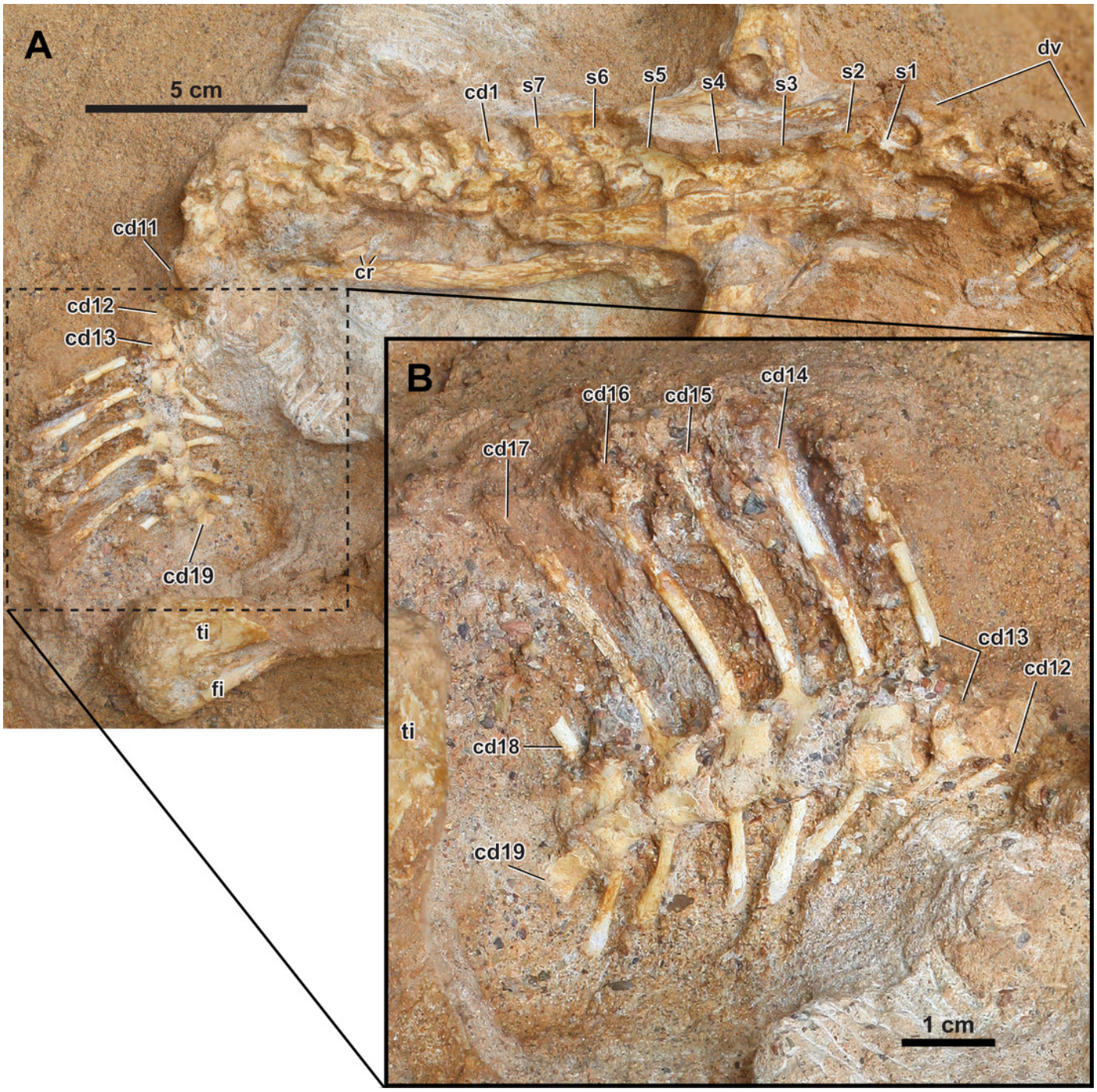
A
5 cm
cd1
s7
s6
s5
s4
s3
s2
s1
dv
cd11
cr
cd12
cd13
cd19
ti
fi
B
cd16
cd15
cd14
cd17
cd13
cd12
ti
cd18
cd19
1 cm

Figure 7

Right appendicular skeleton of *Yamaceratops dorngobiensis* (MPC-D 100/553).

(A) Forelimb in ventrolateral view; (B) Pelvic girdle and hind limb in lateral view. Abbreviations: dpc, deltopectoral crest; f, femur; fi, fibula; ft, fourth trochanter; gt, greater trochanter; h, humerus; ra, radius; u, ulna. L, bones on the left side; lt, lesser trochanter; R, bones on the right side; ti, tibia; ico, inner condyle of the tibia; il, ilium; is, ischium.

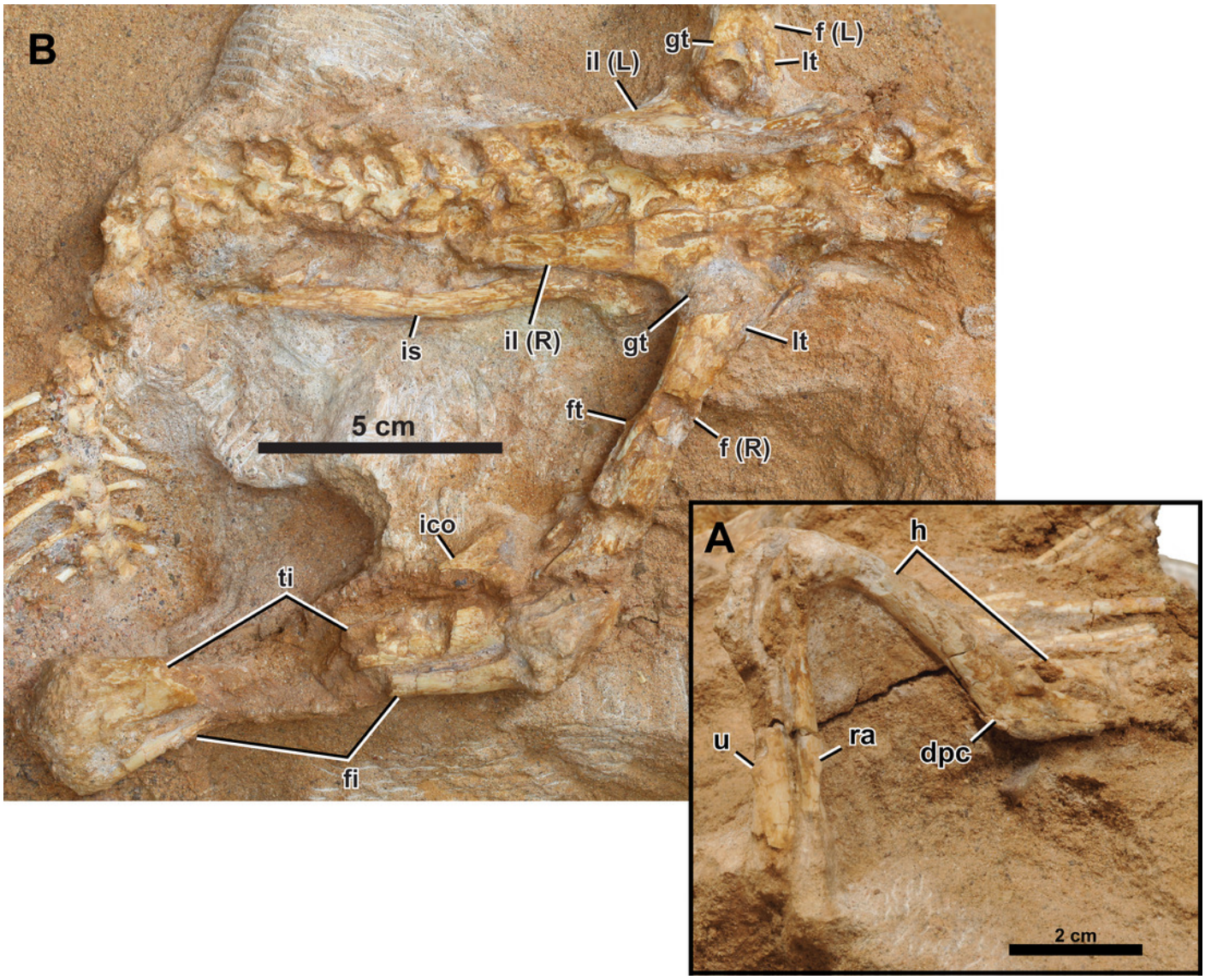

Figure 8

Left appendicular skeleton of *Yamaceratops dorngobiensis* (MPC-D 100/553).

(A) Ilium and pes in lateral view; (B) Pes in dorsal view. Abbreviations: f, femur; ft, fourth trochanter; gt, greater trochanter; L, bones on the left side; lt, lesser trochanter; mt, metatarsal; R, bones on the right side; il, ilium; I, pedal digit I; II, pedal digit II; III, pedal digit III.

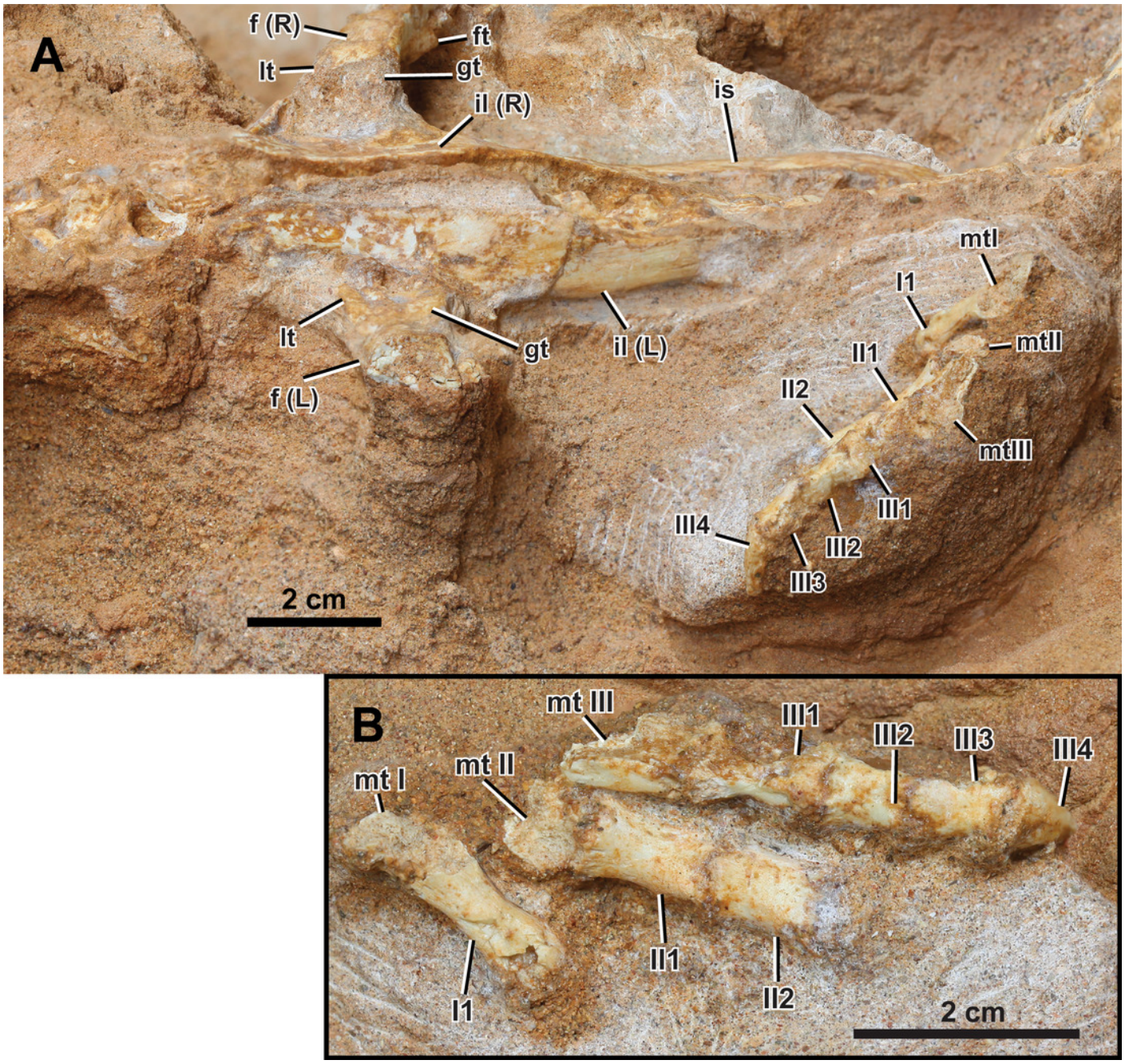
A
f (R)
ft
lt
gt
il (R)
is
mtI
I1
lt
gt
il (L)
mtII
II1
II2
f (L)
mtIII
III1
III4
III2
III3
2 cm
B
mt III
III1
III2
III3
III4
mt I
mt II
II1
II2
I1
2 cm

Figure 9

Histological section of the right humeral shaft of *Yamaceratops dorngobiensis* (MPC-D 100/553).

Three LAGs are traced in white lines.

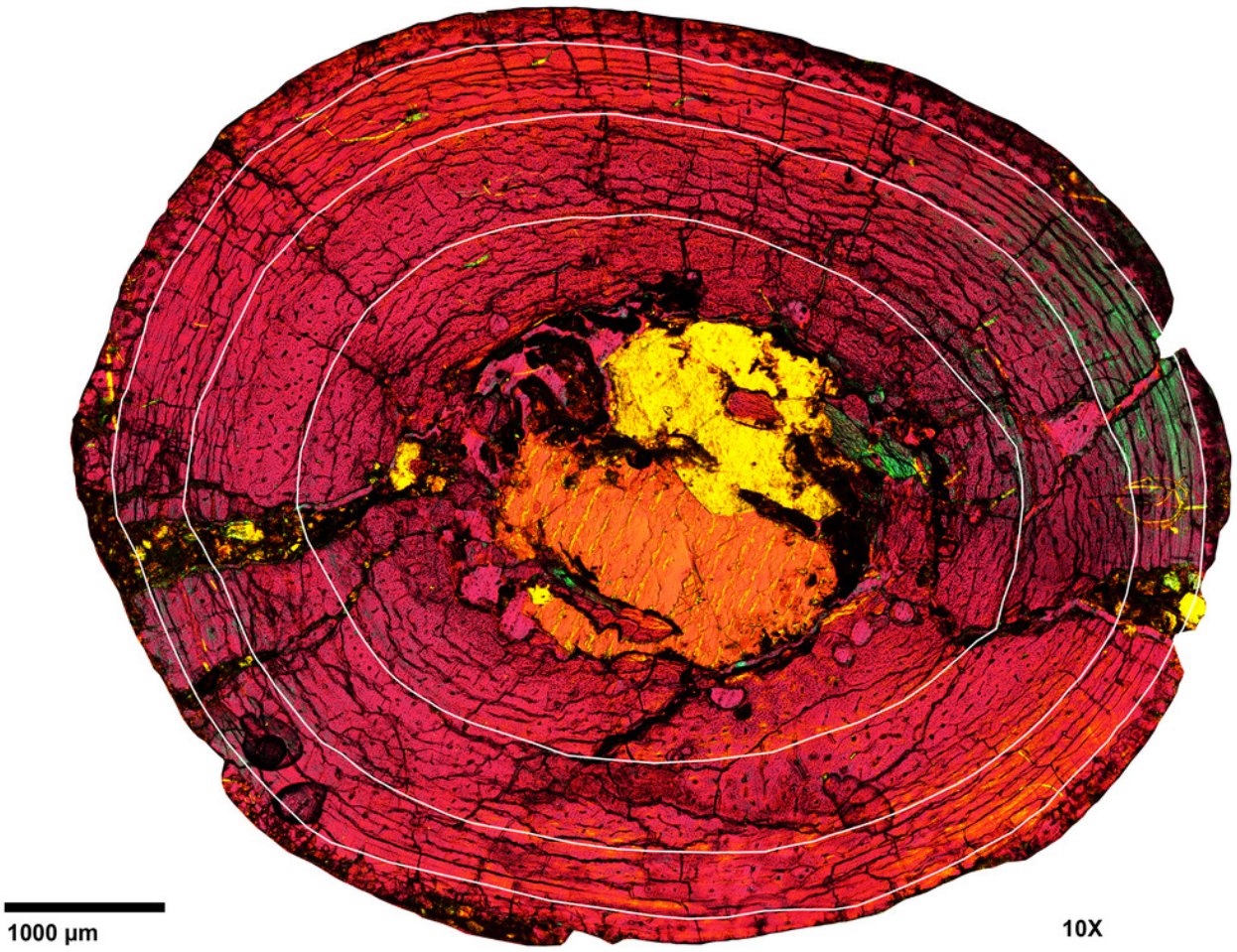

Figure 10

Phylogenetic relationships of *Yamaceratops dorngobiensis* among ceratopsians using the Arbour and Evans (2019) matrix.

Strict consensus tree constructed by using the character matrix of Arbour and Evans (2019) (iteration of the Morschhauser et al. (2018c) matrix) with updated scorings for *Yamaceratops dorngobiensis* and ontogenetically variable characters unscored in taxa represented solely by juvenile specimens. Taxa with middle caudal neural spines about or more than four times longer than the centrum height are highlighted as red color. Numbers at each node indicate Bremer support values.

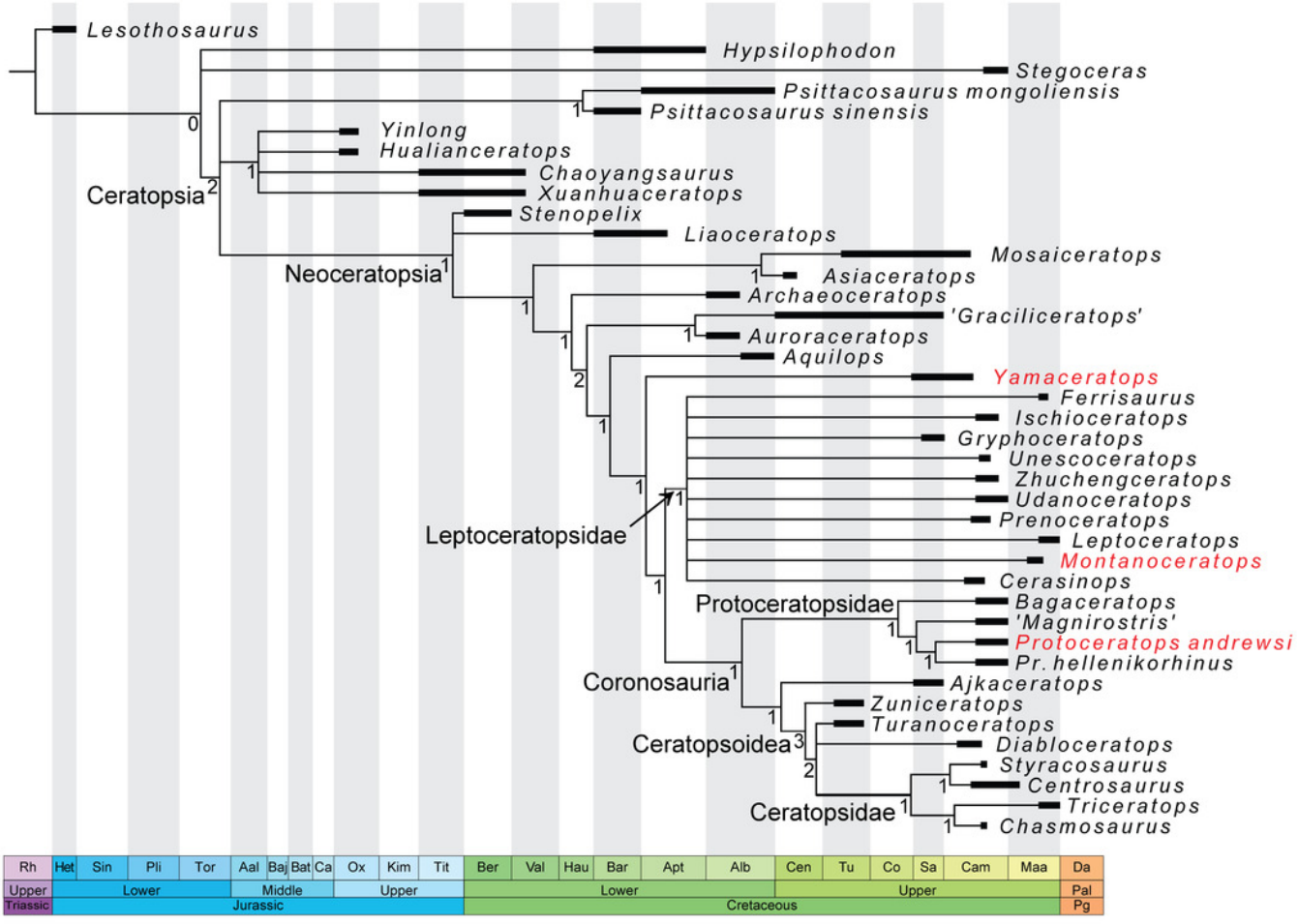

Figure 11

Phylogenetic relationships of *Yamaceratops dorngobiensis* among ceratopsians using the Yu et al. (2020) matrix.

Strict consensus tree constructed by using the character matrix of Yu et al. (2020) (iteration of the Knapp et al. (2018) matrix) with updated scorings for *Yamaceratops dorngobiensis*. *Yamaceratops dorngobiensis* is highlighted as red color. Numbers at each node indicate Bremer support values.

Figure 12

Taphonomy of MPC-D 100/553.

(A) Photograph of the outcrop at the fossil locality. Red star indicates the position where MPC-D 100/553 was found; (B) Photograph of MPC-D 100/553 exposed at the flank of a hill as found, during the excavation; (C) MPC-D 100/553 (skull removed) and its underlying matrix with bedding preserved. The white lines mark the boundary between coarse- and fine-grained sandstone.


A
B
C
carbonate cementation
trough cross-bedding
gleying
5 cm